8-2012

# Studies of Regolithic Vestan Samples: Brecciated Eucrites and Howardites

Sheryl A. Singerling
ssingerl@utk.edu

To the Graduate Council:

I am submitting herewith a thesis written by Sheryl A. Singerling entitled "Studies of Regolithic Vestan Samples: Brecciated Eucrites and Howardites." I have examined the final electronic copy of this thesis for form and content and recommend that it be accepted in partial fulfillment of the requirements for the degree of Master of Science, with a major in Geology.

Harry Y. McSween, Jr., Major Professor

We have read this thesis and recommend its acceptance:

Larry A. Taylor, Josh P. Emery

Accepted for the Council:
Dixie L. Thompson

Vice Provost and Dean of the Graduate School

(Original signatures are on file with official student records.)

# Studies of Regolithic Vestan Samples: Brecciated Eucrites and Howardites

A Thesis Presented for the Master of Science Degree
University of Tennessee, Knoxville

Sheryl A. Singerling
August 2012

## ACKNOWLEDGEMENTS

I thank the following individuals for guidance and support throughout the duration of this project: Hap McSween, my superb adviser; committee members, Larry Taylor, Josh Emery, and Duck Mittlefehldt; lab technicians, Allan Patchen and Luca Fedele; Tim McCoy and Jean-Alix Barrat, for helpful feedback; my colleagues and friends, Andrew Beck, Andrea Patzer, Brian Balta, Yang Liu, Arya Udry, Gregory Drewek, Adam Sarafian, Kevin Thaisen, Richard Cartwright, Latisha Brengman, and Chloe Beddingfield; my family; and EPS graduate students and staff. This work was partly funded by NASA Cosmochemistry grants NNX10AH48G to HYM and NNX11AG58G to LAT.

# ABSTRACT

Brecciated eucrites and howardites represent samples of the regolith of asteroid 4 Vesta. As such, they are a valuable source of data for understanding the products of surface alteration. Two different processes are investigated here: impact mixing of comminuted rocks to produce regolith samples, and formation of glasses in the regolith.

Chapter 1 describes four newly discovered eucrite breccias: three presumably paired meteorites, all named NWA 6105, and NWA 6106. For each meteorite, major- and minor-element compositions of minerals were determined using the electron microprobe. Pyroxene Fe-Mn co-variations and bulk-rock oxygen isotope compositions confirm their classification as eucrites. Variations in mineral compositions and textures are attributed to differences in clast types present (i.e., basaltic or cumulate eucrite). The pyroxene compositions support the hypothesis that samples NWA 6105,1; 6105,2; and 6105,3 are paired polymict eucritic breccias, whereas sample NWA 6106 is a monomict basaltic eucritic breccia. Two-pyroxene geothermometry yields temperatures too low for igneous crystallization. The variation in temperatures among samples suggests that metamorphism occurred prior to brecciation.

Chapter 2 is an investigation of glasses in eight howardites, with the aim of distinguishing their origins as impact melt or pyroclastic. Although theoretical calculations predict that pyroclastic eruptions could have taken place on Vesta, the occurrence of pyroclastic glasses in HED meteorites has never been documented. This study involved petrographic examination of textures, electron microprobe analysis of major and minor elements, and LA-ICP-MS analysis for selected trace elements. Previously documented textural and compositional differences between lunar impact melt and pyroclastic glasses partly guided this study. This work yielded no positive identification of pyroclastic glasses. The most likely explanations are that pyroclastic glasses never formed, either because Vesta contains insufficient volatiles to have powered explosive eruptions, or because eruptive conditions produced optically dense fire-fountains which produced deposits that accumulated in lava ponds. The impact-melt glasses were grouped (K-rich, low-alkali, and Ca-rich) based on compositions. The K-rich group is postulated to result from impacts into previously unsampled, feldspar-rich lithologies, while the low-alkali and Ca-rich glasses are the result of impacts onto known HED lithologies though the latter formed from a preferential melting of plagioclase.

# TABLE OF CONTENTS

# LIST OF TABLES



\

# LIST OF FIGURES

# INTRODUCTION

Meteorites that can be traced to their original parent body are of particular importance, because geologic context allows for a more thorough understanding of formational and evolutionary processes. The only class of asteroidal meteorites that can presently be assigned a specific parent body are the howardite-eucrite-diogenite (HED) achondrites, which are thought to have been derived from the second most massive asteroid, 4 Vesta.

Vesta has a mean radius of 258±12 km, a volume of ~$7.19 \times 10^7 \pm 0.87 \times 10^7$ $km^3$, and a mass of $2.59 \times 10^{20}$ kg (Russell et al., 2012). Due to its large size and the fact that it has experienced magmatic differentiation, Vesta has been referred to as the smallest terrestrial planet (Keil, 2002). Links between Vesta and the HED group have been made based on similarities in reflected spectra (e.g., McCord et al., 1970; Drake, 1979) and the discovery of spectrally similar small bodies (Vestoids) orbiting between Vesta and nearby resonances that act as escape hatches from the main belt (Binzel and Xu, 1993). Similar oxygen isotopic compositions for the different lithologies that comprise the HEDs also indicate a common origin (e.g., Clayton, 2004; Scott et al., 2009) and support extensive melting (Greenwood et al. 2005).

Vesta's differentiation yielded different suites of rock types, possibly corresponding to depth within the asteroid. Moving from the upper mantle or lower crust towards the surface on Vesta, there are diogenites, eucrites, and howardites (Takeda, 1997; Beck and McSween, 2010; Beck, 2011). Most diogenites are coarse-grained cumulates of orthopyroxene (orthopyroxenitic diogenites) (Mittlefehldt, 1994; Keil, 2002; McSween et al., 2011). A few diogenites are harzburgites composed of orthopyroxene and olivine (Beck and McSween, 2010), and at least one is a dunite (Beck et al., 2011). Most are breccias, composed either of orthopyroxenite or of orthopyroxenite-harzburgite mixtures. The eucrites are composed mostly of pyroxene (primarily pigeonite, with minor augite) and plagioclase, with minor ilmenite, troilite, chromite, silica phases and/or silica-rich glass, and Fe-Ni metal (Keil, 2002; Mayne et al., 2009; McSween et al., 2011). They represent shallower lithologies and are divided into two groups based on their environment of crystallization. Cumulate eucrites are coarse-grained gabbros with magnesian pyroxenes that crystallized in plutons, and basaltic eucrites are fine-grained rocks with ferroan pyroxenes that erupted on their parent body's surface or were emplaced in sills and dikes (Keil, 2002). However, most eucrite samples are brecciated and can be distinguished as monomict (clasts from a single eucrite lithology) or polymict (clasts from multiple eucrite lithologies). Howardites are brecciated mixtures of diogenite and eucrite that formed on or near the parent body surface (McSween et al., 2010). The focus of this thesis involves the surficial layer of Vesta—its regolith.

The regolith of any planetary body, particularly one without an atmosphere, represents the boundary between the surface and the space environment. Space weathering is a term that collectively describes processes, both physical and chemical, operating at the surface of an airless body. These processes include comminution (shattering, pulverizing) by impacts as well as irradiation by solar-wind and galactic/cosmic particles (Anand et al., 2004). Several authors have noted that space weathering on Vesta is different from that seen on other bodies, such as the Moon (e.g., Pieters et al., 2012). By studying the products of space weathering on Vesta (i.e., samples of its regolith) we can better understand the mechanisms that generated its unique characteristics. Both brecciated eucrites and howardites represent materials from Vesta's regolith. These two meteorite types are the focus of this thesis.

The first chapter is a multi-authored paper (other authors include A. L. Modi, B. F. McFerrin, E. A. Worsham, H. Y. McSween, L. A. Taylor, D. Rumble, and R. Tanaka) that deals with polymict and monomict eucrite breccias. My role in the paper involved a detailed petrologic

and geochemical study of one of the samples (NWA 6105,3), compilation of data from the other 3 samples, geothermometry calculations, and writing the paper. The paper provides basic petrographic descriptions of four new finds (three, presumably paired NWA 6105 samples, and NWA 6106) from Northwest Africa (Morroco), all recovered in close proximity. The co-variations of Fe and Mn in pyroxenes, as well as the bulk-rock oxygen isotopic compositions, confirm the classification of these samples as eucrites. The textures and compositions of the major minerals (i.e., pyroxene and plagioclase) suggest that samples 6105,1 and 6105,2 contain both basaltic and cumulate eucritic clasts, whereas sample 6105,3 contains multiple basaltic eucrite clasts; all three meteorites are polymict breccias. Sample 6106 contains clasts from a single basaltic eucrite source, so it is a monomict breccia. Equilibration temperatures calculated using two-pyroxene geothermometry are the result of thermal metamorphism rather than igneous crystallization, and these indicate metamorphism occurred prior to assembly of the breccias.

The second chapter is a multi-authored paper (other authors include H. Y. McSween and L. A. Taylor) that investigates 56 glasses in 8 different howardite thin-sections in an attempt to determine their mode of formation (i.e., as impact-melt clasts or as pyroclastic glasses). The other authors provided edits and guidance. Of the glasses analyzed, none had compositions and textures consistent with a pyroclastic origin. Compositionally based glass groupings of impact-melt clasts described by other workers (Barrat et al., 2012) were also investigated, yielding 3 groups: K-rich, low-alkali, and Ca-rich. The K-rich group is unlike any HED compositions known and is inferred to perhaps represent previously unsampled feldspar-rich lithologies on Vesta, while the low-alkali and Ca-rich groups formed from impacts onto HED-like lithologies.

## References


Anand M., Taylor L. A., Nazarov M. A., Shu J., Mao H. K., and Hemley R. J. 2004. Space weathering on airless planetary bodies: Clues from the lunar mineral hapkeite. *Proceedings of the National Academy of Sciences*101:6847-6851.

Beck A. W. and McSween H. Y. 2010. Diogenites as polymict breccias composed of orthopyroxenite and harzburgite. *Meteoritics & Planetary Science* 45:850-872.

Beck A. W. 2011. Petrology and Geochemistry of olivine-bearing diogenites and a group of paired howardites. Ph.D. dissertation, University of Tennessee, Knoxville, TN, USA.

Beck A. W., Mittlefehldt D. W., McSween H. Y., Rumble D., Lee C.-T. A., and Bodnar R. J. 2011. MIL 03443, a dunite from Asteroid 4 Vesta: Evidence for its classification and cumulate origin. *Meteoritics & Planetary Science* 46:1133-1151.

Binzel R. P. and Xu S. 1993. Chips off of Asteroid 4 Vesta; Evidence for the parent body of basaltic achondrite meteorites. *Science* 260:186-191.

Clayton R. N. 2004. Oxygen isotopes in meteorites. In: Davis A. M., editor. *Treatise on geochemistry*. Oxford: Elsevier. pp. 129-142

Drake M. J. 1979. Geochemical evolution of the eucrite parent body: Possible nature and evolution of Asteroid 4 Vesta. In: Gehrels T. and Matthews M. S., editors. *Asteroids*. Tucson: University of Arizona Press. pp. 765-782.

Greenwood R. C., Franchi I. A., Jambon A. ,and Buchanan P. C. 2005. Widespread magma oceans on asteroidal bodies in the early solar system. *Nature* 435:916-918.

Keil K. 2002. Geological history of asteroid 4 Vesta: the "smallest terrestrial planet". In: W. Bottke, A. Cellino, P. Paolicchi, and R. Binzel, editors. *Asteroids III*. Tuscon: Arizona LPI Publishing, pp. 573-585.

Mayne R. G, McSween H. Y, McCoy T. J, and Gale A. 2009. Petrology of the unbrecciated eucrites. *Geochimica et Cosmochimica Acta* 73:794-819.

McCord T. B., Adams J. B., and Johnson T. V. 1970. Asteroid Vesta; spectral reflectivity and compositional implications. *Science* 168(3938):1445-1447.

McSween H. Y., Mittlefehldt D. W., Beck A. W., Mayne R. G., and McCoy T. J. 2011. HED meteorites and their relationship to the geology of Vesta and the Dawn mission. *Space Science Reviews* 163:141-174, doi:10.1007/s11214-010-9637-z.

Mittlefehldt D. W. 1994. The genesis of diogenites and HED parent body petrogenesis. *Geochimica et Cosmochimica Acta* 58:1537-1552.

Pieters C. M. et al. 2012. Space weathering on 4 Vesta: Processes and products. *Abstracts of Papers Presented to the Lunar and Planetary Science Conference* 43: Abstract 1254.

Russell C. T. et al. 2012. Dawn at Vesta: Testing the protoplanetary paradigm. *Science* 336:684-688.

Scott E., Greenwood R. C., Franchi I. A., and Sanders I. S. 2009. Oxygen isotopic constraints on the origin and parent bodies of eucrites, diogenites, and howardites. *Geochimica et Cosmochimica Acta* 73(19):5835-5853.

Takeda H., Ishii T., Arai T., and Miyamoto M. 1997. Mineralogy of the Asuka 87 and 88 eucrites and crustal evolution of the HED parent body. *Antarctic Meteorite Research* 10:401-413.

# CHAPTER 1
# TWO NEW EUCRITE BRECCIAS FROM NORTHWEST AFRICA

## 1. INTRODUCTION

HED meteorites represent the most extensive suite of achondrite samples from a proto-planetary body, generally accepted to be asteroid 4 Vesta based on spectroscopic similarities and orbital constraints (e.g., McCord et al., 1970; Drake, 1979; Binzel and Xu, 1993). Eucrites, the "E" in the HEDs (howardites-eucrites-diogenites), are basalts or gabbros and are believed to have crystallized as surficial lavas or within plutons at shallow crustal levels. Minerals present include pyroxenes and plagioclase as the dominant phases and smaller amounts of troilite, chromite, ilmenite, silica or silica-rich glass, Fe-Ni metal, and phosphate (e.g., Stolper, 1977; Mittlefehldt et al., 1998; Keil, 2002; McSween et al., 2011). Depending on texture and mineral composition, the eucrites are subdivided into basaltic and cumulate eucrites. Basaltic eucrites are fine- to medium-grained with Fe-rich, exsolved pyroxenes with fine lamellae (zoned or not, depending on whether they have suffered later thermal metamorphism) and plagioclase of $An_{75-96}$. Cumulate eucrites are coarse-grained with Mg-rich exsolved pyroxenes with coarse lamellae and plagioclase of $An_{90-96}$ (e.g., Delaney and Prinz, 1984; Mittlefehldt et al., 1998; McSween et al., 2011). Eucrites are often brecciated and occur as either monomict (having only one pyroxene type) or polymict (having two or more pyroxene types) rocks. Characteristics of the pyroxene types are outlined in detail elsewhere (i.e., Miyamoto et al., 1978; Delaney et al., 1982).

The focus of this study involves two newly discovered eucrite breccias represented by four meteorites: NWA 6105,1 (~12 g), 6105,2 (~1 g), 6105,3 (~9 g), and 6106 (~302 g); all were recovered in near proximity in Morocco. The purpose of this study is to provide classifications and petrographic descriptions for all four meteorites. Previous work on these samples was only preliminary and reported in abstracts (McFerrin et al., 2010; Singerling et al., 2011). By analyzing these new eucrites, we can provide a more representative sampling of these basaltic lithologies on Vesta, which is essential to a better understanding of Vestan magmatic processes.

## 2. METHODS

Polished thin-sections of the four meteorites were observed with a petrographic microscope to describe their mineralogy and petrography. The imaging software *Infinity Analyze* was used to construct maps of the samples in reflected light at 2.5x magnification. Areas of interest were also imaged in plane-polarized and cross-polarized light at higher magnifications. Modal abundances were established using *ImageJ* (free image analysis software) on BSE (back-scattered electron) images, following the method outlined by Liu et al. (2009). Mineral compositions were determined using the wavelength dispersive spectrometers (WDS) of the CAMECA SX-100 electron microprobe (EMP) analyzer. These analyses were performed with an accelerating potential of 15 keV, a beam current of 20 nA (10 nA for feldspars and glass), and a 1-5 µm beam size (10 µm for plagioclase). Peak and background counting times were 20 sec. Detections limits (3σ above background) were as follows: 0.03 wt% for $SiO_2$, $TiO_2$, $Al_2O_3$, $Cr_2O_3$, MgO, MnO, and CaO; 0.05 wt% for FeO, $Na_2O$ and $K_2O$; and 0.05-0.1 wt% for Co and Ni in metal.

Oxygen isotope analyses were performed with a laser-fluorination vacuum-preparatory line and MAT 253 mass spectrometer at ISEI. The $\delta^{18}O$ measurements were calibrated against VSMOW, which was fluorinated in the same vacuum-preparatory line and analyzed on the same mass spectrometer. The $\delta^{17}O$ analyses were calibrated based on the analysis of terrestrial silicate minerals as $\Delta^{17}O = 0$, where $\Delta^{17}O = 1000 \times [\ln(\delta^{17}O/1000+1) - 0.527 \times \ln(\delta^{18}O/1000+1)]$

(Miller, 2002). The $\delta^{18}O$ of reference garnet material, UWG-2 (Valley et al., 1995), gives a value of 5.65 ‰ relative to VSMOW. Analytical precision (1σ, N = 6), based on replicate analysis of UWG-2 garnet, is ± 0.03 ‰ for $\delta^{17}O$, ± 0.05 ‰ for $\delta^{18}O$, and ± 0.024 ‰ for $\Delta^{17}O$.

## 3. RESULTS

### 3.1 Petrographic Descriptions

*3.1.1 NWA 6105,1*

NWA 6105,1 is a breccia containing numerous eucrite clasts (Fig. 1a). The mineral modes (vol.%) of the sample are: pyroxene (low- and high-Ca) 56 %, plagioclase 43 %, with ilmenite, troilite, chromite, Fe-Ni metal, phosphate, and glass each <1 %. The pyroxenes in the matrix are predominately pigeonite with some grains having fine exsolution lamellae of augite. Shock effects are relatively common, causing fractures and undulatory extinction in plagioclase and pyroxene grains. Opaque minerals include angular chromite and ilmenite. Most of the minor minerals are enclosed by low-Ca pyroxenes; however, some grains occur as fragments within the matrix and as grains interstitial to pyroxene and plagioclase in clasts. The grain sizes of matrix minerals range from <5 μm to 4 mm.

Within the matrix of NWA 6105,1, there are numerous eucrite clasts (7 identified in our thin section), varying in size, composition, and texture. The clasts range in size from 1-5 mm and vary in shape from round to angular; they tend to be medium-grained and resemble cumulate eucrites, although their pyroxene compositions are not magnesian enough (Mittlefehldt et al., 1998). All the clasts contain large pyroxene and plagioclase grains surrounded by a fine-grained clastic matrix. The clasts vary in texture from ophitic to hypidiomorphic granular and are predominately hypocrystalline containing crystals of pigeonite and plagioclase, within a matrix of pyroxene, plagioclase, opaque phases, phosphate, and in some cases, glass. Most of the pyroxene grains are pigeonite, with exsolution lamellae of augite ~5-15 μm thick.

*3.1.2 NWA 6105,2*

NWA 6105,2 is a breccia within a breccia, composed of two distinct lithologies, A and B, which make up ~75 % and ~25 % of the sample, respectively (Fig. 1b). The larger fragment A is coarse-grained with ophitic to subophitic clasts. The modes for the clast are: pyroxene (low- and high-Ca) 55 %, plagioclase 40 %, and matrix 5 %. Individual clast sizes are typically 0.5-1 mm. The majority of the pigeonite grains are moderately fractured. Most of the plagioclase grains are twinned and show undulatory extinction. Evidence of shock metamorphism includes bent twin-lamellae, mosaicism, and pervasive fractures in plagioclase, although no maskelynite was observed. Ilmenite and chromite are non-uniformly distributed within fragment A, occurring as large (~50-100 μm) anhedral grains within the matrix or as irregular blebs or elongate rods in pigeonite grains.

The smaller lithic fragment B is fine-grained and shares many textural similarities with NWA 6105,1. The modes in this clast are: pyroxene (low- and high-Ca) 54 %, plagioclase 38 %, silica 8 %, with ilmenite, troilite, chromite, and Fe-Ni metal, each <1 %. The matrix of B is enriched in glass and opaque phases which cause it to appear darker.

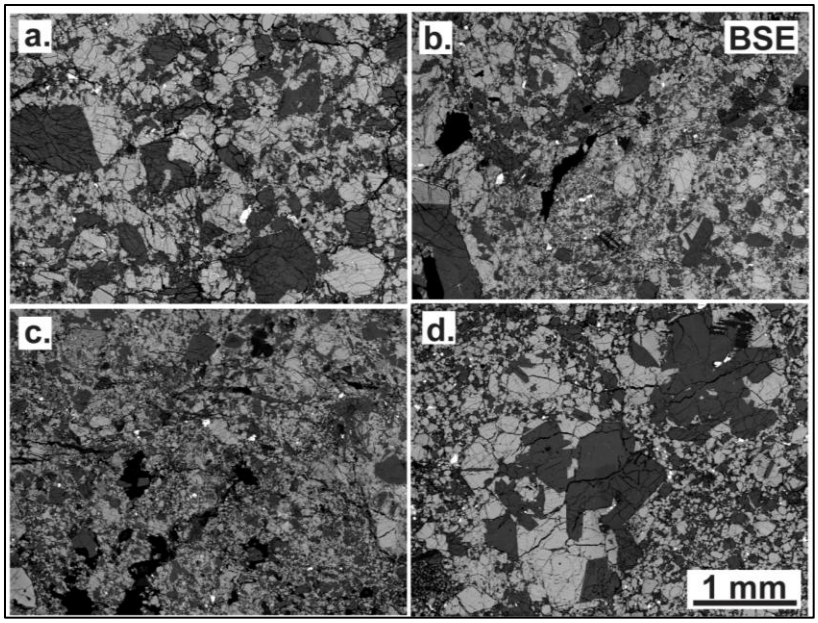

**Figure 1.** Backscattered electron (BSE) images of thin sections (a) NWA 6105,1; (b) 6105, 2; (c) 6105, 3; and (d) 6106. All images are at the same scale.

*3.1.3 NWA 6105,3*

NWA 6105,3 is a fine-grained eucrite breccia with textures indicative of shock metamorphism (Fig. 1c). There are 2 distinctive clasts: one brecciated and one sulfide-rich.. The modes of the sample are: pyroxene (low- and high-Ca) 51 %, plagioclase 30 %, silica 15 %, calcite 4 %, with ilmenite, troilite, chromite, and Fe-Ni metal, each <1 %. The pyroxene grains are subhedral to euhedral and range in size from <5-250 μm. The <5-50 μm pyroxene grains in the matrix are granoblastic polygonal, with exsolution. The largest (~300 μm) pyroxene clast, located near the center of the thin section, displays slightly different compositions from the rest of the pyroxenes in the sample. This is referred to as 6105,3 Clast in the figures and tables in later portions of the paper. Plagioclase ranges from crystalline to polycrystalline grains to maskeleynite. These grains range in size from 10 μm to 0.5 mm in the matrix. Ilmenite, troilite, chromite, and Fe-Ni metal occur as euhedral or anhedral grains that range in size from <5-130 μm. They are dispersed throughout the sample, with the exception of the sulfide-rich clast characterized by anhedral troilite blebs. Silica occurs as anhedral grains that range in size from <5 μm to 0.2 mm. Using Ca X-ray maps, calcite was also observed as a secondary (terrestrial alteration) mineral present in fractures along one edge of the sample.

*3.1.4 NWA 6106*

NWA 6106 is a breccia containing unbrecciated igneous lithic clasts (7 identified) which have an ophitic to subophitic texture (Fig. 1d). The modes of this sample are: pyroxene (low- and high-Ca) 47 %, plagioclase 48 %, silica 3 %, with calcite, ilmenite, troilite, chromite, and Fe-Ni metal, each <1%. The pyroxenes contain exsolution lamellae ranging in apparent thickness from <5-12 μm and are subhedral to anhedral. Pyroxenes range in size from <0.1-1.7 mm. The chromite, ilmenite, and metal grains are anhedral, ranging from <0.1-0.3 mm. The plagioclase is

mostly lath-shaped with Carlsbad and albite twinning. The grain-size ranges from <0.1 mm in the crushed matrix to ~0.8 mm in some lithic clasts. A vein, which was determined to be calcite with the EMP, cuts through the thin section and is interpreted as a product of terrestrial weathering.

## 3.2 Mineral Compositions

### *3.2.1 Pyroxene*

NWA 6105 and 6106 are breccias, and as such it should come as no surprise that they have significant variations in the major-element compositions of pyroxene and plagioclase. Representative analyses were chosen to illustrate the ranges of compositions of pyroxene and plagioclase. The results for each sample are listed in Table 1.

Variations in pyroxenes mainly occur in Ca-content and, to a lesser extent, Mg- and Fe-content. Fig. 2 shows pyroxene quadrilaterals for all analyzed pyroxene compositions in the four meteorites. Ternary diagrams of minor elements (Ti-Al-Cr) are included as well. As the pyroxene composition becomes more Ca-rich, it also becomes less Fe-rich. The trend observed here was also reported by Mayne et al. (2009) and is termed the Ca-Fe trend. Finely exsolved pyroxenes cause what appears to be a continuous range in composition along the Ca-Fe trend. In reality, the pyroxenes are either high-Ca (exsolved augite lamellae) or intermediate- to low-Ca (host pigeonite). The limitations of instrument resolution cause what appear to be intermediate compositions.

Pyroxenes in NWA 6105,1 and 6105,2 (Fig. 2a and b) show two distinct Ca-Fe trends, one anchored at ~$En_{50}$ and another at ~$En_{40}$. These are symbolized according to the type of eucrite clast: cumulate (open circles) versus basaltic (closed circles). NWA 6105,1 shows more variation in the $En_{50}$ trend, which may reflect several different cumulate compositions in this sample. NWA 6105,3 also has pyroxenes with several trends, as shown in Fig. 2c and d; one trend is characteristic of the groundmass pyroxenes ($En_{40}$), and the other represents analyses of a single, large (~300 μm) pyroxene clast ($En_{46-40}$). NWA 6106 has only one Ca-Fe trend ($En_{36}$), as shown in Fig. 2e. The variety of these major-element trends in pyroxenes reflect different formational histories (i.e., parent magmas, degree of thermal metamorphism, etc.)

Minor elements such as Ti, Al, and Cr equilibrate more slowly than major elements in pyroxenes, so one can expect a greater spread in these data even after thermal metamorphism (Mayne et al., 2009). Fig. 2 shows ternary diagrams of these three elements. Two trends are present, as described by Mayne et al. (2009): (1) constant Ti and variation in Cr-Al, as illustrated in Fig. 2c; (2) constant Cr and variation in Ti-Al, as illustrated in Fig. 2d. The other diagrams show mixtures of these two trends. There appears to be no consistent pattern among minor elements that distinguishes cumulate and basaltic eucrite clasts.

### *3.2.2 Plagioclase*

Plagioclase shows a range of compositions for the analyzed grains in each meteorite sample (Table 1). Fig. 3 shows portions of an An-Ab-Or ternary diagram, depicting the compositions of plagioclase. The heterogeneous compositions of the plagioclase imply that it is not equilibrated in terms of major-elements, unlike the pyroxenes. Plagioclase takes more time than pyroxene does to equilibrate in terms of major elements (Mayne et al., 2009).

**Table 1.** Representative major- and minor-element data from electron microprobe analyses (oxides in wt. %, cations in nb ions).

| NWA 6105,1 | Opx† | | Augite† | | Plag† | | NWA 6105,2 | Opx† | | Augite† | | Plag† | |
|---|---|---|---|---|---|---|---|---|---|---|---|---|---|
| | Cum | Basaltic | Cum | Basaltic | Core | Rim | | Cum | Basaltic | Cum | Basaltic | Core | Rim |
| **$SiO_2$** | 50.9 | 49.0 | 51.0 | 52.1 | 44.4 | 46.3 | **$SiO_2$** | 51.1 | 49.6 | 51.4 | 50.1 | 44.7 | 49.1 |
| **$TiO_2$** | 0.28 | 0.10 | 0.39 | 0.18 | <0.03 | <0.03 | **$TiO_2$** | 0.15 | 0.19 | 0.71 | 0.48 | <0.03 | <0.03 |
| **$Al_2O_3$** | 0.33 | 0.41 | 1.02 | 0.60 | 34.8 | 33.8 | **$Al_2O_3$** | 0.57 | 0.24 | 1.41 | 0.68 | 35.4 | 32.7 |
| **$Cr_2O_3$** | <0.03 | 0.56 | <0.03 | 0.15 | <0.03 | <0.03 | **$Cr_2O_3$** | 0.48 | 0.23 | 0.42 | 0.60 | <0.03 | <0.03 |
| **MgO** | 17.9 | 12.3 | 13.7 | 11.3 | <0.03 | <0.03 | **MgO** | 17.0 | 12.5 | 13.4 | 11.1 | <0.03 | <0.03 |
| **CaO** | 0.53 | 0.65 | 20.4 | 21.5 | 18.9 | 17.4 | **CaO** | 0.56 | 2.26 | 20.5 | 15.0 | 18.6 | 15.7 |
| **MnO** | 0.86 | 1.13 | 0.44 | 0.41 | <0.03 | <0.03 | **MnO** | 0.98 | 1.08 | 0.44 | 0.72 | <0.03 | <0.03 |
| **FeO** | 29.1 | 35.5 | 12.2 | 13.6 | 0.58 | 0.14 | **FeO** | 29.5 | 33.9 | 11.8 | 21.1 | 0.43 | 0.29 |
| **$Na_2O$** | <0.05 | <0.05 | <0.05 | 0.06 | 0.61 | 1.57 | **$Na_2O$** | <0.05 | <0.05 | <0.05 | <0.05 | 0.69 | 2.57 |
| **$K_2O$** | <0.05 | <0.05 | <0.05 | <0.05 | <0.05 | 0.14 | **$K_2O$** | <0.05 | <0.05 | <0.05 | <0.05 | 0.10 | 0.11 |
| **Total** | 100.1 | 99.8 | 100.3 | 100.0 | 99.3 | 99.3 | **Total** | 100.3 | 100.1 | 100.1 | 99.8 | 99.9 | 100.5 |
| | | | | | | | | | | | | | |
| **Ox Basis** | 6 | 6 | 6 | 6 | 8 | 8 | | 6 | 6 | 6 | 6 | 8 | 8 |
| **Si** | 1.966 | 1.970 | 1.942 | 1.985 | 2.069 | 2.144 | **Si** | 1.971 | 1.978 | 1.938 | 1.955 | 2.068 | 2.235 |
| **Ti** | 0.008 | 0.003 | 0.011 | 0.005 | n.d. | n.d. | **Ti** | 0.004 | 0.006 | 0.020 | 0.014 | n.d. | n.d. |
| **Al** | 0.015 | 0.019 | 0.046 | 0.027 | 1.911 | 1.844 | **Al** | 0.026 | 0.011 | 0.063 | 0.031 | 1.929 | 1.757 |
| **Cr** | n.d. | 0.018 | n.d. | 0.004 | n.d. | n.d. | **Cr** | 0.015 | 0.007 | 0.013 | 0.019 | n.d. | n.d. |
| **Mg** | 1.034 | 0.739 | 0.775 | 0.644 | n.d. | n.d. | **Mg** | 0.981 | 0.741 | 0.756 | 0.644 | n.d. | n.d. |
| **Ca** | 0.022 | 0.028 | 0.830 | 0.879 | 0.943 | 0.866 | **Ca** | 0.023 | 0.096 | 0.829 | 0.629 | 0.92 | 0.766 |
| **Mn** | 0.028 | 0.038 | 0.014 | 0.013 | n.d. | n.d. | **Mn** | 0.032 | 0.036 | 0.014 | 0.024 | n.d. | n.d. |
| **Fe** | 0.940 | 1.193 | 0.388 | 0.435 | 0.023 | 0.005 | **Fe** | 0.953 | 1.131 | 0.372 | 0.689 | 0.017 | 0.011 |
| **Na** | n.d. | n.d. | n.d. | 0.004 | 0.055 | 0.141 | **Na** | n.d. | n.d. | n.d. | n.d. | 0.062 | 0.227 |
| **K** | n.d. | n.d. | n.d. | n.d. | n.d. | 0.009 | **K** | n.d. | n.d. | n.d. | n.d. | 0.006 | 0.007 |
| **Total** | 4.017 | 4.009 | 4.019 | 3.996 | 5.004 | 5.009 | **Total** | 4.004 | 4.008 | 4.005 | 4.007 | 5.001 | 5.003 |

**Table 1. Continued**

| NWA 6105,3 | Opx† | Augite† | Plag† | | NWA 6106 | Opx† | Augite† | Plag† | |
|---|---|---|---|---|---|---|---|---|---|
| | pyx3b | pyx16a | Core | Rim | | LC1 | LC4 | Core | Rim |
| **$SiO_2$** | 49.9 | 50.4 | 44.7 | 48.5 | **$SiO_2$** | 48.9 | 51.3 | 45.2 | 48.0 |
| **$TiO_2$** | 0.15 | 0.49 | <0.03 | <0.03 | **$TiO_2$** | 0.29 | 0.25 | <0.03 | <0.03 |
| **$Al_2O_3$** | 0.15 | 0.78 | 35.2 | 32.8 | **$Al_2O_3$** | 0.33 | 0.57 | 35.1 | 32.5 |
| **$Cr_2O_3$** | 0.08 | 0.39 | <0.03 | <0.03 | **$Cr_2O_3$** | 0.13 | 0.26 | <0.03 | <0.03 |
| **MgO** | 13.1 | 10.9 | <0.03 | <0.03 | **MgO** | 11.1 | 11.1 | <0.03 | <0.03 |
| **CaO** | 3.00 | 18.2 | 18.4 | 15.9 | **CaO** | 2.25 | 19.9 | 18.8 | 16.4 |
| **MnO** | 1.02 | 0.61 | <0.03 | <0.03 | **MnO** | 1.10 | 0.53 | <0.03 | <0.03 |
| **FeO** | 32.4 | 18.0 | 0.09 | 0.13 | **FeO** | 35.8 | 15.8 | 0.09 | 0.22 |
| **$Na_2O$** | <0.05 | 0.06 | 0.89 | 2.24 | **$Na_2O$** | <0.05 | <0.05 | 0.94 | 2.02 |
| **$K_2O$** | <0.05 | <0.05 | <0.05 | 0.37 | **$K_2O$** | <0.05 | <0.05 | <0.05 | 0.21 |
| **Total** | 99.8 | 99.9 | 99.2 | 99.9 | **Total** | 99.84 | 99.76 | 100.1 | 99.4 |
| | | | | | | | | | |
| **Ox Basis** | 6 | 6 | 8 | 8 | | 6 | 6 | 8 | 8 |
| **Si** | 1.982 | 1.935 | 2.076 | 2.222 | **Si** | 1.974 | 1.957 | 2.082 | 2.215 |
| **Ti** | 0.004 | 0.018 | n.d. | n.d. | **Ti** | 0.008 | 0.014 | n.d. | n.d. |
| **Al** | 0.007 | 0.038 | 1.926 | 1.774 | **Al** | 0.016 | 0.017 | 1.908 | 1.770 |
| **Cr** | 0.003 | 0.026 | n.d. | n.d. | **Cr** | 0.004 | 0.028 | n.d. | n.d. |
| **Mg** | 0.775 | 0.625 | n.d. | n.d. | **Mg** | 0.665 | 0.666 | n.d. | n.d. |
| **Ca** | 0.128 | 0.751 | 0.915 | 0.779 | **Ca** | 0.097 | 0.088 | 0.927 | 0.811 |
| **Mn** | 0.034 | 0.018 | n.d. | n.d. | **Mn** | 0.038 | 0.037 | n.d. | n.d. |
| **Fe** | 1.074 | 0.601 | 0.003 | 0.005 | **Fe** | 1.207 | 1.223 | 0.003 | 0.008 |
| **Na** | n.d. | 0.004 | 0.08 | 0.199 | **Na** | n.d. | n.d. | 0.084 | 0.181 |
| **K** | n.d. | n.d. | n.d. | 0.022 | **K** | n.d. | n.d. | n.d. | 0.013 |
| **Total** | 4.009 | 4.016 | 5.003 | 5.001 | **Total** | 4.008 | 4.019 | 5.007 | 4.997 |

†representative analyses
n.d. = not detected; Cum = cumulate

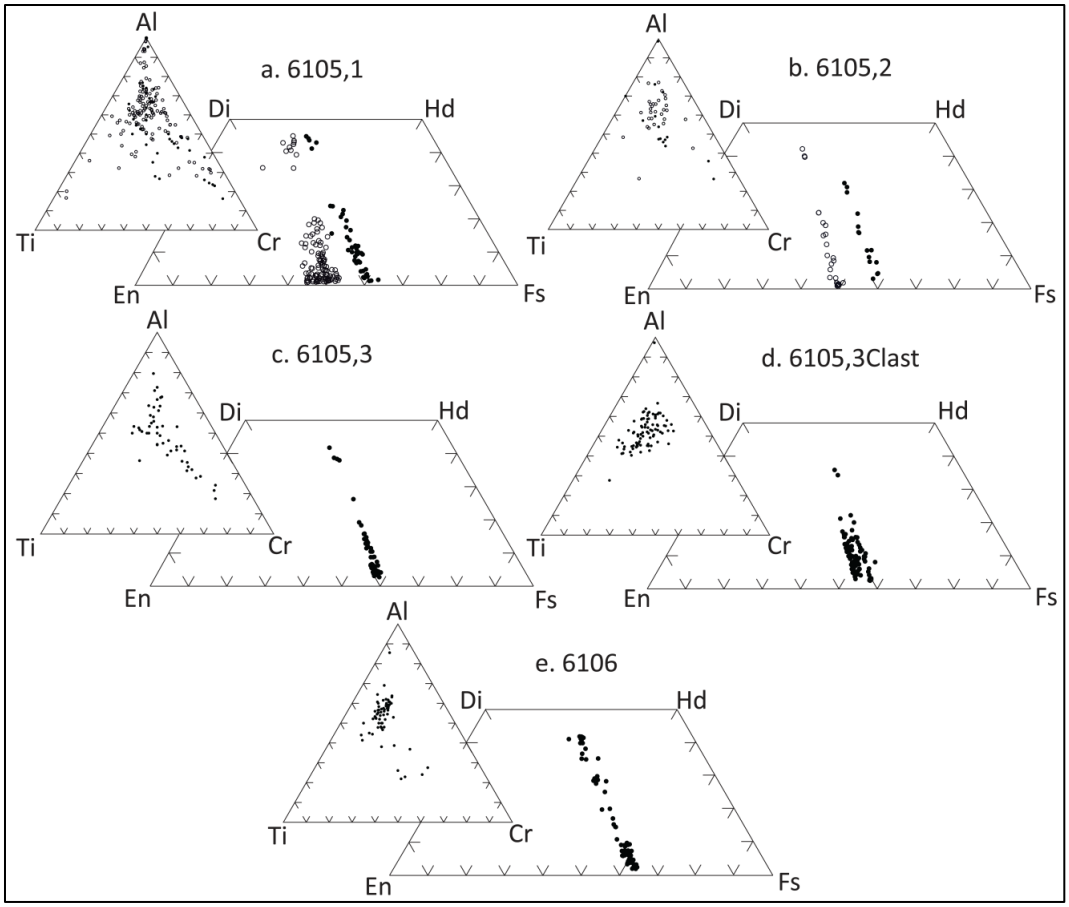


**Figure 2.** Pyroxene quadrilaterals and minor-element ternary diagrams for (a) NWA 6105,1; (b) 6105,2; (c) 6105,3; (d) 6105,3Clast; and (e) 6106. Open circles=cumulate eucrite; closed circles=basaltic eucrite.

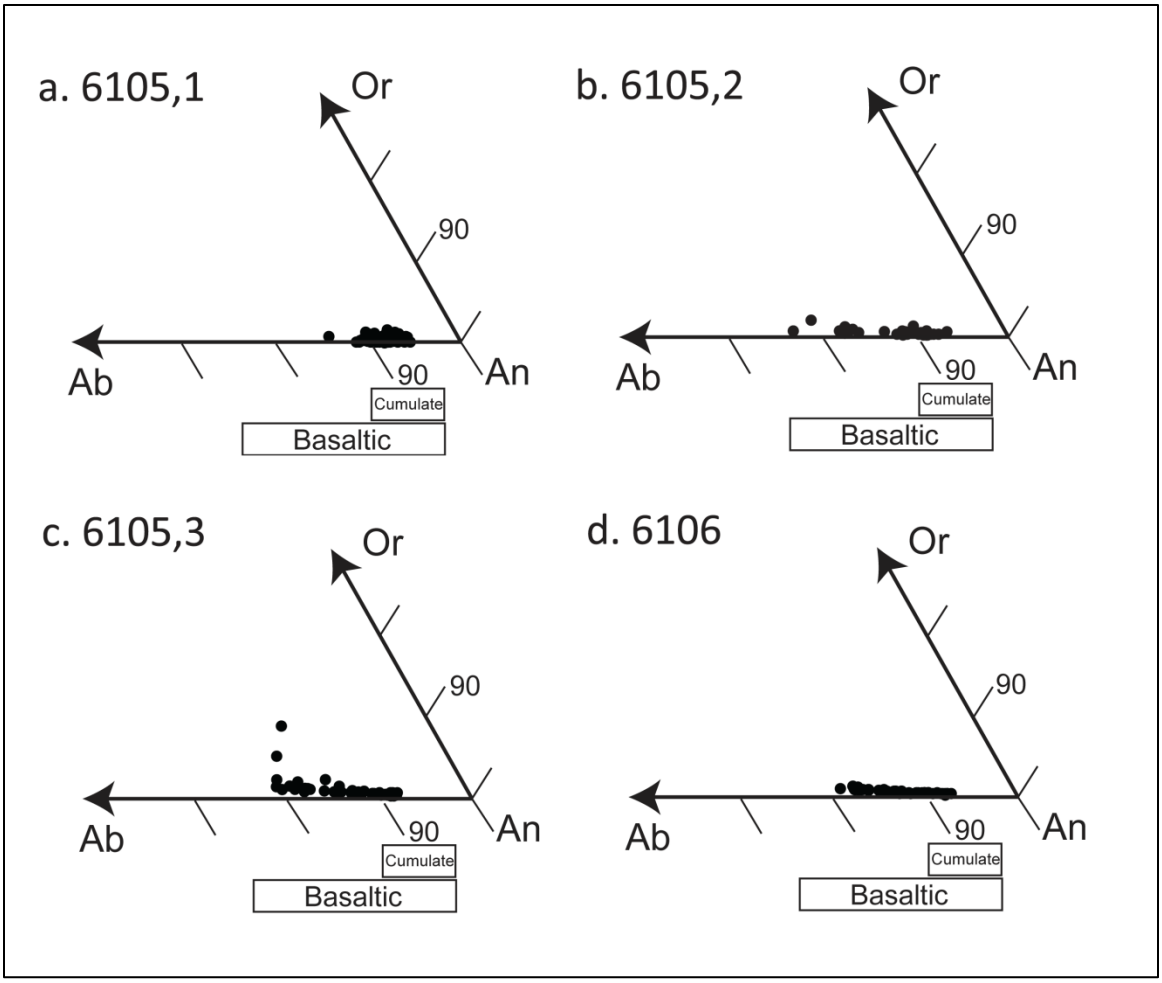


**Figure 3.** An-Ab-Or ternary diagram depicting the plagioclase compositions in (a) NWA 6105,1; (b) 6105,2; (c) 6105,3; and (d) 6106. Basaltic and cumulate envelopes labeled (Mayne et al., 2009; McSween et al., 2011).

## 4. DISCUSSION

### 4.1 Classification

Data obtained from electron microprobe analysis can aid in quantitatively determining the classification of these samples as eucrites. A useful method involves plotting Mn versus Fe in pyroxenes (Fig. 4). The figure includes reference lines for Vesta, Earth, and the Moon (Papike et al., 2003; Lentz et al., 2007).

Oxygen isotopes are also useful in identifying the parent body of a given meteoritic sample. Table 2 lists oxygen isotope data, and Fig. 5 illustrates these values for the NWA samples studied. All samples plot approximately along the HED mass-fractionation line.

### 4.2 Geothermometry

The QUILF (quartz-ulvospinel-ilmenite-fayalite) two-pyroxene geothermometer (Andersen et al., 1993) was used to estimate the equilibration temperatures of NWA 6105 and 6106. The exsolution lamellae of augites in host orthopyroxenes are suitable for geothermometry. Normally, the QUILF two-pyroxene geothermometer requires known Ca-contents of coexisting augite-orthopyroxene and the orientation of the two-pyroxene tie-line. For this work, the end-members were chosen for the cumulate and basaltic pyroxene trends within samples containing both clast types, because the pyroxene values form discrete mixing lines for each trend. The QUILF program uses En and Wo values for augite-orthopyroxene pairs to calculate the equilibration temperatures. The data used for the calculations, as well as the equilibration temperatures obtained, are summarized in Table 3.

The determined temperatures, in all cases, are too low to reflect igneous crystallization which requires crystallizations from a melt; for eucrites, this occurs at ~1060°C (Stolper, 1977). Instead, the calculated temperatures likely resulted from thermal metamorphism. The temperatures do not closely agree for the basaltic clasts in the NWA 6105 samples (6105,1 = 645 ±32; 6105,2 = 886 ±39; and 6105,3 = 814 ±46 °C) indicating that metamorphism likely occurred before breccia assembly. It is important to note that the temperature obtained for NWA 6105,1 is very low for a basaltic eucrite. In fact, it is lower than the temperature calculated for the cumulate clasts (652 ±52°C) in this sample.

Some of the equilibration temperatures are in agreement with values reported in the literature within standard error. The exceptions include both basaltic and cumulate clasts in NWA 6105,1 and cumulate clasts in NWA 6105,2. Typical basaltic eucrite equilibration temperatures range from 800-950°C (Delaney et al., 1984) with a more complete range of 700-1000°C (Yamaguchi, 1996). For a comparison to other Vestan lithologies, the cumulate eucrite range is 765-992°C, while the diogenite range is 719-840°C (Harlow et al., 1979; Takeda et al., 1976; Mittlefehldt, 1994). The fact that some of the NWA 6105 temperatures lie outside of literature values means some clasts of this sample experienced extremely slow cooling. While the equilibration temperatures have two values for the NWA 6105 samples (~660°C and ~850°C), reflecting their polymict nature, the temperature for NWA 6106 is distinct (722°C).

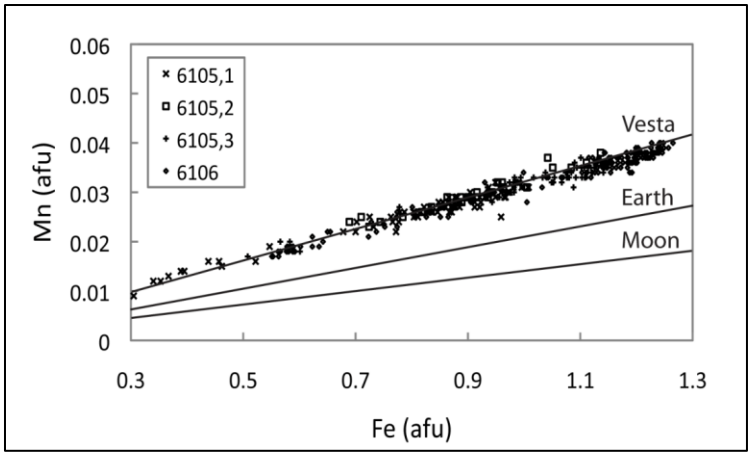


**Figure 4.** Mn versus Fe contents of pyroxenes plot along the bold Vesta line defined by other HEDs (Papike et al., 2003; Lentz et al., 2007) within standard error.

**Table 2.** Oxygen isotope data for NWA 6105,1; 6105,3; and 6106. The data are in good agreement with the HEDFL.

| **Sample** | **$\Delta^{17}O$** | **$\delta^{17}O$** | **$\delta^{18}O$** |
|---|---|---|---|
| **NWA 6105,1** | -0.255 | 1.71 | 3.74 |
| | -0.237 | 1.77 | 3.80 |
| **NWA 6105,3** | -0.223 | 1.83 | 3.91 |
| | -0.239 | 1.76 | 3.80 |
| **NWA 6106** | -0.237 | 1.75 | 3.77 |
| | -0.264 | 1.78 | 3.88 |
| **Average** | -0.243 | 1.77 | 3.82 |
| **Standard Dev** | 0.015 | 0.04 | 0.06 |

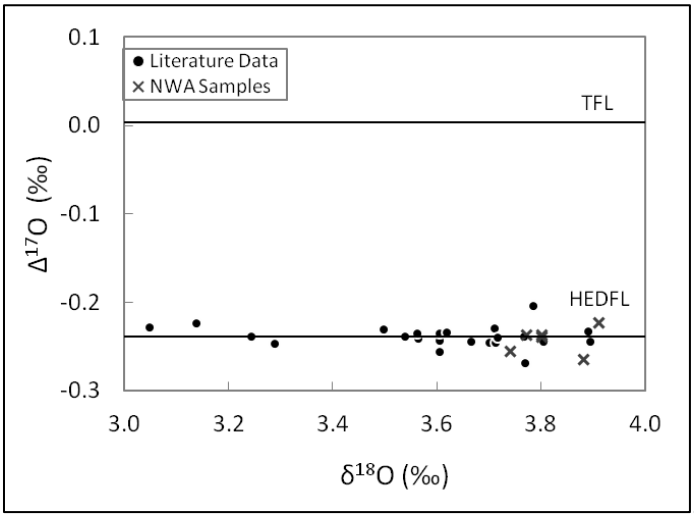


**Figure 5.** Oxygen isotope plot illustrating that NWA 6105 and 6106 (gray x's) are HEDs. The terrestrial fractionation line (TFL) is plotted for reference. Data are from Greenwood et al. (2005) and Franchi et al. (1999).

**Table 3.** Geothermometry data used for QUILF program and equilibration temperatures for NWA samples.

| | | 6105,1 | | 6105,2 | | 6105,3 | 6105,3Clast | 6106 |
|---|---|---|---|---|---|---|---|---|
| | | **Cum** | **Bas** | **Cum** | **Bas** | **Bas** | **Bas** | **Bas** |
| **Augite** | **En (%)** | 36.3 | 32.9 | 38.6 | 32.8 | 32.3 | 33.1 | 29.4 |
| | **Wo (%)** | 45.0 | 44.9 | 42.4 | 32.1 | 41.8 | 36.0 | 41.8 |
| **Opx** | **En (%)** | 54.8 | 38.2 | 50.2 | 39.8 | 38.8 | 40.5 | 35.6 |
| | **Wo (%)** | 0.81 | 1.33 | 1.08 | 3.23 | 2.83 | 2.60 | 1.96 |
| **T (°C)** | | 652±52 | 645±32 | 684±32 | 886±39 | 814±46 | 828±40 | 722±30 |

Cum = cumulate
Bas = basaltic

### 4.3 Pairing

The NWA 6105 and 6106 samples were all found in close proximity, which may suggest pairing. If paired, these samples should display similar textures and mineral compositions. We also might expect the temperatures of equilibration to be similar, but the brecciated nature of the samples makes the utility of this characteristic questionable.

The pyroxene compositions and textures indicate that samples NWA 6105,1; 6105,2; and 6105,3 are polymict eucritic breccias containing either cumulate and basaltic clasts or basaltic clasts of differing compositions. The Ca-Fe trends of each are essentially equivalent (cumulate clasts with $En_{50}$ and basaltic with $En_{40}$) with the exception of the large pyroxene clast ($En_{46-40}$) in 6105,3 which falls in between the two trends on the pyroxene quadrilateral. Although no cumulate eucrite clasts were found in 6105c, it is clearly polymict and cumulate clasts may occur in a larger sample. Sample NWA 6106, on the other hand, is a monomict basaltic eucritic breccia. NWA 6106 has different textures and pyroxene compositions (Ca-Fe trend of $En_{36}$) than any of the 6105 samples. The geothermometry results provides further evidence of pairing.The NWA 6105 samples have two distinct values, indicating their polymict nature, while the NWA 6106 sample has one value that is distinct from either of the temperatures obtained for 6105.

A combination of the above evidence implies that the NWA 6105 samples are paired though only further work, such as determining cosmic-ray exposure ages, can truly determine whether this is indeed the case. The evidence also suggests that the NWA 6105 samples and the NWA 6106 sample are not paired.

## 5. CONCLUSIONS

The following points summarize our findings related to NWA 6105 and 6106:

- All four meteorites are breccias composed of eucrite clasts set in a finely comminuted matrix.
- Classification of these meteorites as eucrites is supported by the pyroxene Mn vs. Fe plot and oxygen isotope data.
- Pyroxene grains in NWA 6105,1 and 6105,2 define two Ca-Fe trends, one basaltic and one cumulate; 6105,3 pyroxenes also define multiple basaltic Ca-Fe trends, both basaltic; and those of 6106 define one basaltic Ca-Fe trend.

- We suggest that NWA 6105,1, 6105,2 and 6105,3 are paired samples of a polymict basaltic/cumulate eucrite breccia, and NWA 6106 is a monomict basaltic eucrite breccia.
- Geothermometry yields temperatures of metamorphic equilibration ranging from ~652-886°C. These temperatures indicate metamorphism before the final assembly of the 6105 breccia.

## References


Andersen D. J., Lindsley D. H., and Davidson P. M. 1993. QUILF: A PASCAL program to assess equilibria among Fe-Mg-Mn-Ti oxides, pyroxenes, olivine, and quartz. *Computers and Geoscience* 19:1333-1350.

Binzel R. P. and Xu S. 1993. Chips off of Asteroid 4 Vesta; Evidence for the parent body of basaltic achondrite meteorites. *Science* 260:186-191.

Delaney J. S. and Prinz M. 1984. The polymict eucrites. *Journal of Geophysical Research* 89:C251-C288.

Delaney J. S., O'Neill C., Nehru C. E., Prinz M. 1982. Zoning of minerals in mafic clasts from basaltic achondrites. *Proc. Lunar Planetary Science Conference* 13:154-155.

Drake M. J. 1979. Geochemical evolution of the eucrite parent body: Possible nature and evolution of Asteroid 4 Vesta. In *Asteroids*, edited by Gehrels T. and Matthews M. S. Tucson: University of Arizona Press., pp. 765-782.

Franchi I. A., Wright I. P., Sexton A. S., and Pillinger C. T. 1999. The oxygen isotopic composition of Earth and Mars. *Meteoritics & Planetary Science* 34:657-661.

Greenwood R. C., Franchi I. A., Jambon A., and Buchanan P. C. 2005. Widespread magma oceans on asteroidal bodies in the early Solar System. *Nature* 435:916-918.

Harlow G. E., Nehru C. E., Prinz M., Taylor G. J., and Keil K. 1979. Pyroxenes in Serra de Mage: Cooling history in comparison with Moama and Moore County. *Earth Planetary Science Letters* 43:173-181.

Keil K. 2002. Geological history of asteroid 4 Vesta: the "smallest terrestrial planet". In *Asteroids III*, edited by W. Bottke, A. Cellino, P. Paolicchi, and R. Binzel. Arizona LPI Publishing,. pp. 573-585.

Lentz R., Scott E., and McCoy T. J. 2007. Anomalous eucrites: Using Fe/Mn to search for different parent bodies. *Proc. Lunar Planetary Science Conference* 37:1968.

Liu Y., Floss C., Day J. M. D., Hill E., and Taylor L. 2009. Petrogenesis of lunar mare basalt meteorite Miller Range 05035. *Meteoritics & Planetary Sciences* 44:261-284.

Mayne R. G., McSween H. Y., McCoy T. J., and Gale A. 2009. Petrology of the unbrecciated eucrites. *Geochimica et Cosmochimica Acta* 73:794-819.

McCord T. B., Adams J. B., and Johnson, T. V. 1970. Asteroid Vesta; spectral reflectivity and compositional implications. *Science* 168:1445-1447.

McFerrin B., Worsham E. A., McSween H. Y., and Taylor L. A. 2010. Petrology of two new eucrites from north west Africa. *Proceedings, 41st Lunar and Planetary Science Conference*. #2381

McSween H. Y., Mittlefehldt D. W., Beck A. W., Mayne R. G., and McCoy T. J. 2011. HED meteorites and their relationship to the geology of Vesta and the Dawn mission. *Space Science Reviews.* 163:141-174, doi:10.1007/s11214-010-9637-z.

Miller, M.F. 2002. Isotopic fractionation and the quantification of $^{17}O$ anomalies in the oxygen three-isotope system: an appraisal and geochemical significance. *Geochimica et Cosmochimica Acta* 66:1881-1889.

Mittlefehldt D. W. 1994. The genesis of diogenites and HED parent body petrogenesis. *Geochimica et Cosmochimica Acta* 58:1537-1552.

Mittlefehldt D. W., McCoy T. J., Goodrich C. A., and Kracher A. 1998. Non-chondritic meteorites from asteroidal bodies. In *Planetary Materials,* 1st ed., edited by Papike J. J. Washington, D.C.: Mineralogical Society of America. pp. 4-1–4-195.

Miyamoto M., Takeda H., Duke M. B., and Yanai K. 1978. Pasamonte-like clasts in eucrite polymict breccias. *Proc. Lunar Planetary Science Conference* 9:744-746.

Papike J. J., Karner J. M., and Shearer C. K. 2003. Determination of planetary basalt parentage: A simple technique using the electron microprobe. *American Mineralogist* 88:469-472.

Singerling S. A., Modi A. L., Taylor L. A., and McSween H. Y. 2011. Polymict eucrites NWA 6105A and 6105B: Paired HEDs. *Proceedings, 42nd Lunar and Planetary Science Conference*. #1207

Stolper E. 1977. Experimental petrology of eucritic meteorites. *Geochimica et Cosmochimica Acta* 41:587-611.

Takeda, H., Miyamoto M., T. Ishii, and Reid A. M. 1976. Characterization of crust formation on a parent body of achondrites and the Moonby pyroxene crystallography and chemistry. *Proc. Lunar Planetary Science Conference* 17:3535-3548.

Valley, J.W., Kitchen, N., Kohn, M.J., Niendorf, C.R., Spicuzza, M.J. 1995. UWG-2, a garnet standard for oxygen isotope ratios: Strategies for high precision and accuracy with laser heating. *Geochimica et Cosmochimica Acta* 59:5223-5231.

Yamaguchi A., Taylor G. J., and Keil K. 1996. Global crustal metamorphism of the eucrite parent body. *Icarus* 124:97-112.

# CHAPTER 2
# GLASSES IN HOWARDITES: IMPACT-MELT CLASTS OR PYROCLASTIC GLASSES?

# 1. INTRODUCTION

Meteorite breccias, which represent near-surface lithologies on airless bodies, often contain glasses. Using the Moon as an analogy, these glasses could potentially be either impact-melt clasts or pyroclastic glasses. Here, we explore the possibility that these two types of melts formed on asteroid 4 Vesta. The textures and compositions of glasses can be quite definitive. They are often minor components of regoliths primarily due to the nature of their genesis—rapid quenching of a melt. In a terrestrial setting, pyroclasts most often occur during fire-fountaining, which takes place in mildly explosive volcanic eruptions. The airborne droplets solidify before falling back to the surface, forming pyroclastic glasses. Another mechanism for producing rapidly quenched melts, not so common on Earth, is shock from hypervelocity micro-meteorite (<1 mm) impacts. Micro-meteorite impacts that form melts are on airless bodies, where impact-melt clasts can accumulate over long time-spans (e.g., Schaal and Horz, 1977; Chapman, 1997; Bell et al., 2002; Horz et al., 2005).

## 1.1 Impact-Melt Clasts

The surfaces of airless bodies are prone to energetic micro-meteorite impacts on small scales not experienced on Earth, because its atmosphere decelerates all but the largest impactors. Projectiles impact at significant speeds, though these speeds are a function of heliocentric distance (Dohnanyi, 1975; Grun et al., 1977). Micro-meteorite impact events that occur on the Moon have an average velocity of 14 km/s, while those that occur between objects in the asteroid belt average 5 km/s (Hartmann, 1977). This difference in velocity causes less melt to be produced from impacts on asteroids than on the Moon (Keil et al. 1997). Following the impact event, the impactor and target material (roughly equivalent in volume to the impactor) are compressed to high pressures resulting in the formation of a shock wave (Pierazzo et al., 1997). The energy released from this compression and subsequent relaxation produces the heat necessary to form impact melt (Melosh and Vickery, 1991). This only occurs in impacts that reach a certain energy threshold. For lower energy impacts, melting primarily occurs at grain boundaries (Schaal et al., 1979). The amount of melt produced depends on multiple factors such as ambient temperature and pressure, gravity, impact velocity, projectile mass, target porosity, target material, shape of the impactor, etc. (Schaal et al., 1979; Vickery and Melosh, 1991; Pierazzo et al., 1997).

When impact melts form, they are often heated to their boiling points, and cooled rapidly enough to form glasses (Fig. 1). Not all minerals have the same impact-melting temperature, so relict grains (if partially melted, they appear to have been "resorbed") are often present in the resulting impact melts, along with a general lack of compositional homogeneity of the glass. At lower energy impacts (20 to 40 GPa presures), feldspar-rich glasses result because feldspar is among the first phases to melt under shock conditions (Schaal et al., 1979; Stoffler et al., 1991), meaning impact melts are often enriched in $SiO_2$ and $Al_2O_3$ compared to the bulk compositions of the target material (Horz et al., 2005). For higher energy impacts, the glass composition approaches that of the bulk rock (Schaal et al., 1979; Horz et al., 2005).

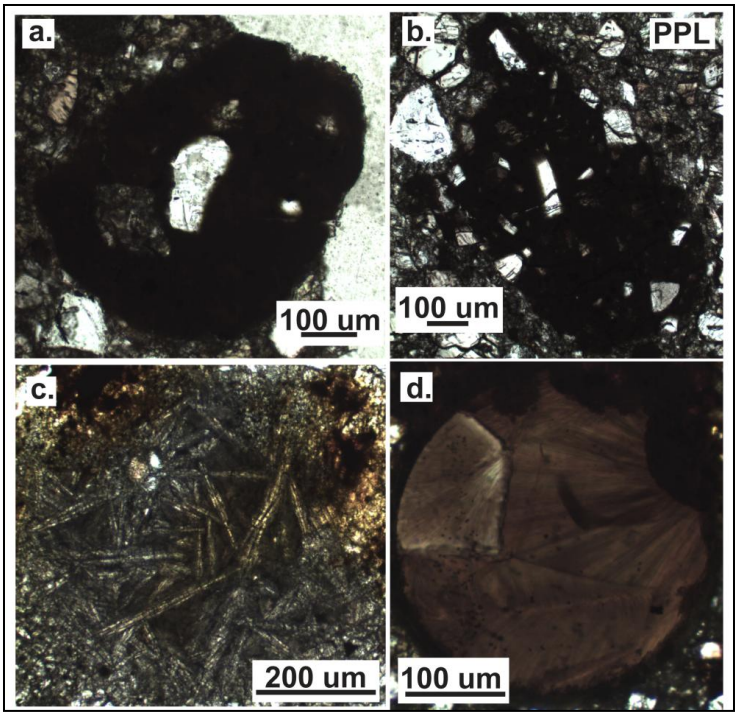


**Figure 1.** Photomicrographs (plane polarized light) of impact-melt clasts in howardite samples. Note the presence of partly resorbed mineral grains and the irregular shapes of both (a) and (b). Quench textures are displayed in (c) and (d).

Other common characteristics of impact-melt glasses include fine-grained textures, formed by rapid crystallization, and high concentrations of siderophile elements (Beck et al., 2011). The latter are due to the nature of the impactor, which is usually chondritic in composition with a significant abundance of metals and sulfides. Impact-metamorphosed breccia clasts share many physical similarities with crystallized impact-melt clasts. This, together with the same environment of formation, make distinguishing between the two rather difficult. Ryder and Spudis (1987) outlined several characteristics common only to impact-melt clasts in lunar breccias that help to differentiate them. These include euhedral/skeletal olivine, bladed ilmenites and ilmenite chains, plagioclase laths, interstitial glass, rounded clasts, vesicles, and heterogeneous mineral compositions. The value of impact-melt clasts lies in their ability to tell us about the geochemistry of the original target materials which, in turn, adds to the lithologic inventory of a planetary body (Delano, 1991).

### 1.2 Pyroclastic Glasses

Pyroclasts are the "individual crystals, crystal fragments, glass fragments, and rock fragments generated by disruption as a direct result of volcanic action" (Schmid, 1981). The formation of pyroclasts is driven by density contrasts which initiate motion of the gases in a magma (Wilson and Head, 1981). The first material erupted at the surface of a body tends to be volatile-rich. As a consequence, it erupts explosively forming features called fire- or lava-fountains. These fire-fountains allow droplets of lava to form, which cool in flight producing glass beads or pyroclastic glasses. The formation of pyroclastic glasses is limited to silicate

planetary bodies which experienced magmatic activity sometime in their past. The Moon is the only body, other than Earth, from which we have documented pyroclastic glass samples. Large asteroids, those big enough to experience differentiation, also had the potential to form pyroclastic glasses.

Asteroid 4 Vesta appears to meet the size qualification for pyroclastic glass retention (Wilson et al., 2010), but pyroclastic material has not yet been definitively identified (Keil, 2002). Pyroclastic glass formation requires magmas containing sufficient volatiles, and it is unlikely that Vesta's magmas were completely volatile-free (Grady et al., 1997a & b; Sarafian et al., 2012). Vesta is an excellent case study due to its large size and abundance of near-surface samples (howardites) that contain glasses.

### 1.3 Howardites

If Vesta experienced violent volcanic eruptions that produced pyroclastic glasses, we could best hope to find such material in howardites. "Regolithic" howardites were on the surface of Vesta. They exhibit enrichment in solar-wind noble gases, higher siderophile (Ni) abundances, and greater proportions of glasses and impactor-chondritic clasts (Warren et al., 2009a, 2009b). The presence of carbonaceous chondrite xenoliths in these breccias cause howardites to exhibit a greater spread about the eucrite-diogenite compositional mixing line than other groups (Wilkening, 1973; Mittlefehldt et al., 1998; Keil, 2002). Glasses in regolithic howardites include impact-glass beads and impact-melt clasts (e.g., Labotka and Papike, 1980; Mittlefehldt and Lindstrom, 1997). The vast majority of howardites are actually "fragmental" rather than "regolithic" (Warren et al, 2009a, 2009b). Members of this group lack the diagnostic characteristics cited above but still represent near-surface samples.

The difficulty of recognizing pyroclastic glasses lies in distinguishing them from the common impact-melt clasts. Here we evaluate chemical and physical characteristics particular to the two glass types in howardites. Extensive work attempting to distinguish impact-melt glasses from pyroclastic glasses has been performed on lunar samples (e.g., Heiken and McKay, 1974, Butler, 1978; Stone et al., 1982; Delano, 1986; Shearer and Papike, 1993; Taylor et al., 2006). In this study, we explore whether the lunar glasses can be used as an analogue for Vestan glasses. Both are small, rocky, airless bodies with low $fO_2$, an abundance of basaltic surficial compositions, and similar depletions of volatile elements (Papike et al. 1998; Taylor et al., 2006; McSween et al., 2011).

The purpose of this work is a study of glasses in howardites with an attempt at addressing two primary questions:

1. Are impact-melt clasts and pyroclastic glasses both present in howardites?
This portion of the chapter is termed "The Search for Pyroclastic Glasses". The value of discovering Vestan pyroclastic glasses lies in the information they might yield on volatile inventory and eruptive conditions.

2. Are there compositional groupings of impact-melt glasses in howardites?
Compositionally unique groups of howardite glasses have been identified by other authors (i.e., Warren et al., 2009b; Barrat et al., 2009a, 2009b, 2012). If these groupings are real, they might represent some lithologies not yet seen on Vesta, adding to its lithologic diversity.

## 2. METHODS

The first stage in this research involved obtaining appropriate meteorite samples. We began by examining several howardite samples recovered from Antarctica that were suggested to possibly contain pyroclastic glasses based on textural features (D. W. Mittlefehldt, personal communication). To this list we added other howardites with high glass contents, as determined by petrographic inspection of the Antarctic howardite collection at the NASA Johnson Space Center. The studied samples are listed in Table 1. Thin sections of these were allocated by the Meteorite Working Group and obtained from NASA's Astromaterials Acquisition and Curation Office. Basic petrographic analyses of glasses were performed with a petrographic microscope. The imaging software *Infinity Analyze* was used to construct sample maps in transmitted and reflected light at 2.5x magnification. Glasses of interest were also imaged in plane-polarized and reflected light at higher magnifications.

Glasses were analyzed for major- and minor-element compositions using the CAMECA SX-100 electron microprobe (EMP) analyzer at the University of Tennessee. Only glasses with minimal crystalline phases were studied. For the glass-grouping portion of this work, each individual probe point was treated as an individual analysis due to heterogeneities within glass clasts. These analyses were performed with wavelength dispersive spectrometers using an accelerating potential of 15 keV, a beam current of 10 nA, and a 5-10 μm diameter beam.

A test for volatilization/mobilization during EMP analyses was performed on a K-rich glass in which we compared values obtained for $Na_2O$ and $K_2O$ at different currents and different beam sizes (test 1 = constant current of 10 nA and variable beam sizes of 10 and 1 μm; test 2 = constant beam size of 10 μm and variable beam currents of 10 and 20 nA). No volatilization was observed, supporting our use of the aforementioned beam currents and sizes (10 nA, and a 5-10 μm). Peak and background counting times were 20s (30s for K and Na). Detection limits (3σ above background) were as follows: 0.02 wt% for $Al_2O_3$; 0.03 wt% for $SiO_2$; 0.04 wt% for MgO, $K_2O$, CaO; 0.05 wt% $TiO_2$; 0.06 wt% for $Na_2O$; 0.07 wt% for FeO; 0.08 wt% $Cr_2O_3$. The number of analyses per glass varied from 5 to 23 depending on its size. Only analyses with wt% totals of 98.5–101 were used.

**Table 1.** Howardite samples used in this study. The glasses studied column includes those imaged for their textures and those analyzed with the electron microprobe. The analyses column refers to the total individual microprobe points measured for the crystalline-free glasses.

| Sample | Glasses Studied | Analyses |
|---|---|---|
| EET 87532,13 | 9 | 25 |
| EET 87509,68 | 7 | 0 |
| EET 87518,12 | 6 | 0 |
| QUE 94200,16 | 12 | 65 |
| PCA 02014,6 | 3 | 0 |
| LAP 04838,19 | 11 | 0 |
| MIL 05085,11 | 7 | 39 |
| MIL 05085,2 | 1 | 23 |

As with major elements, each individual analysis was treated as its own glass sample for trace elements. Trace-element compositions were determined using an Agilent 7500ce ICP-MS combined with an Excimer 193 nm ArF GeoLasPro LA system at Virginia Polytechnic Institute and State University. Depending on the sizes of the glass samples, beam sizes ranged from 16-32 μm and dwell times from 30-40 sec. For an external standard, NIST 610 glass was used a total of four times before and after each analysis. For an internal standard, all elements were summed to 100%. Analysis Management System (AMS) software was used for data reduction with a 3σ LOD (Mutchler et al., 2008). The accuracy and precision of the analyses were 2-5 % relative (Norman et al., 1996).

## 3. THE SEARCH FOR PYROCLASTIC GLASSES

### 3.1 Criteria for Discriminating Between Lunar Glass Origins

Considerable study of lunar glasses has resulted in several criteria, both physical and chemical, that can be used in tandem to determine the likelihood of a particular glass being of pyroclastic origin. Delano (1986) identified these as follows:

1. Absence of partly resorbed clasts and schlieren (swirly texture, Fig. 2).
   Both these textures are indicative of impact melts and represent pre-existing heterogeneities in the target material.
2. Intra-sample chemical homogeneity for the nonvolatile elements (e.g., Ti, Al, Cr, Fe, Mn, Mg, Ca, and REEs). These element abundances should be relatively consistent in a pyroclastic glass.
3. Inter-sample chemical homogeneity and/or fractionation trends.
   This constraint applies to multiple pyroclastic glasses.
4. High Mg/Al ratio compared to the lunar regolith.
   This constraint is due to the former existence of a global magma ocean. The source material of the pyroclastic glasses is Al-depleted due to the formation of the anorthositic highlands.
5. Mg-correlated Ni abundances.
   Ni acts as a compatible element in olivine, and so Mg and Ni show a correlation.

The previous five criteria apply to glasses in thin section and/or grain mounts. The following two criteria only apply to whole grains; consequently, they are not useful as a proxy for Vestan glasses since our study was limited to *in situ* techniques.

6. Surface coatings of volatile elements.
7. Ferromagnetic resonance intensity.

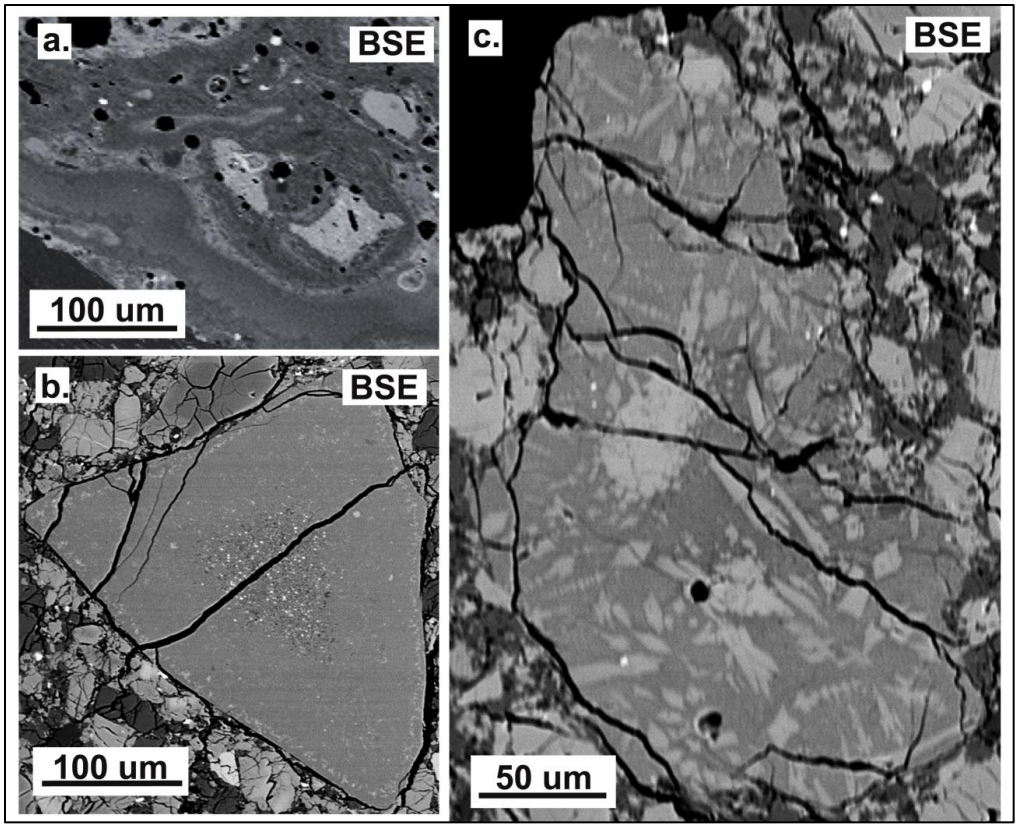


**Figure 2.** Textures typical of impact-melt clasts: (a) schlieren, (b) Fe or sulfide "dust" in the center of the glass, and (c) partly resorbed clasts. (a) from Apollo 11 10084 courtesy of Yang Liu, (b) from QUE 94200,16, and (c) from EET 87509,68.

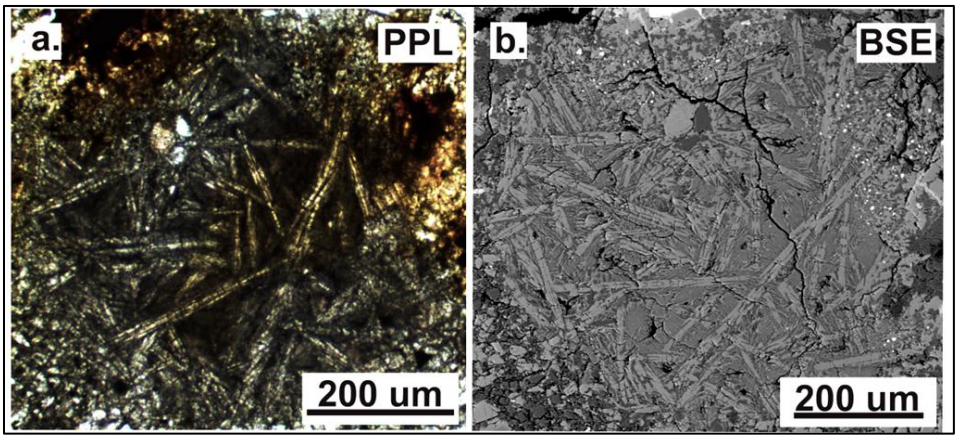


**Figure 3.** Skeletal texture of a glass in EET 87532,13 in (a) plane polarized light and (b) as a backscatter electron image.

The most important criterion is intra-sample chemical homogeneity of the glass. If a glass does not meet this criterion, we can automatically assume that it is not pyroclastic in origin. Still, other criteria have some merit as well. Analyzing the textures of impact-melt clasts and pyroclastic glasses is a qualitative method for distinguishing the origin of a given sample. Both represent materials formed by rapid quenching which produces vitric (glassy), vitrophyric (glassy with small phenocrysts), dendritic (tree-like crystal growth), or skeletal (Fig. 3) textures. Impact melts often contain incompletely melted clasts (relict grains/partly resorbed clasts) and metal/sulfide dust grains (Fig. 2c), whereas pyroclastic glasses may contain phenocrysts but are most often just glass. Still, impact-melt clasts can also be entirely devoid of crystalline phases, making the textural distinction between pyroclastic glasses and impact-melt clasts difficult. Therefore, chemical homogeneity of the glass is paramount.

The primary cause of textural differences between pyroclastic glasses and impact-melt clasts involves the different mechanisms of formation. Impact-melt clasts form as a result of shock, and so one would expect relict minerals to exhibit indicators of shock. These might be (i) dislocations, planar microstructures (PFs and PDFs), mechanical twins, kink bands, and mosaicism; (ii) high-pressure phase transformations; (iii) decomposition into two or more phases; and (iv) partial melting and vaporization (Langenhorst, 2002). Shapes typical of pyroclastic glasses include spheres, oblate and prolate spheroids, teardrops, shards, and irregular shapes (Stone et al., 1982). Impact-melt clasts are often angular or amoeboidal and can form very large clasts, relative to pyroclastic glasses.

Differences in texture between the two glass types are less diagnostic than differences in composition and so the two should, ideally, be used in conjunction. A shock origin causes lunar impact-melt clasts to lose alkalis and other volatile elements (Ivanov and Florensky, 1975; Jeanloz and Ahrens, 1976; Naney et al., 1976; Delano et al., 1981; Fudali et al., 1984; Vaniman, 1990; Keller and McKay, 1991, 1992; Papike et al. 1997). Chemical characteristics common to lunar pyroclastic glasses are higher MgO and lower $Al_2O_3$ and CaO abundances in comparison to most fine-grained non-cumulate mare basalts (Shearer and Papike, 1993), volatile concentrations equal to or less than those of mare basalts (Papike et al. 1998), and enrichment in the following elements in comparison to mare basalts: Br, Zn, Tl, Ag, Pb, Sb, Bi, Au, and Cu (Chou et al., 1975; Wasson et al., 1976; Delano, 1986; Taylor et al., 2006).

### 3.2 Criteria for Discriminating Between Vestan Glass Origins

Textural features of each lunar glass type are expected to hold for Vestan samples, but this is not the case for compositional features. The most important criteria for pyroclastic glasses, intra-sample homogeneity, holds for Vesta, but not all chemical differences between lunar impact-melt clasts and pyroclastic glasses apply to Vestan samples. This is due to fundamental differences between the two bodies (e.g., different internal pressures, lithologies, formational histories, etc). For example, the low Mg/Al ratios of impact-melt clasts as compared to mare basalts and pyroclastic glasses on the Moon can be explained by the presence of the anorthositic highlands. The mantle source for pyroclastic glasses on the Moon is Al-depleted because it is complementary to the anorthositic crust. This is not the case on Vesta, where the crust has a basaltic, rather than anorthositic composition. Table 2 summarizes the pivotal characteristics that ought to hold for samples from Vesta.

**Table 2.** Textural and chemical differences between impact-melt clasts and pyroclastic glasses on Vesta.

| | Impact-Melt Clasts | Pyroclastic Glasses |
|---|---|---|
| **Texture** | - vitric/vitrophyric<br>- dendritic/skeletal<br>- vesicles<br>- partly resorbed clasts<br>- schlieren<br>- metals/sulfide "dust" | - vitric/vitrophyric<br>- dendritic/skeletal<br>- vesicles |
| **Composition** | - intra-sample heterogeneity | - intra-sample homogeneity |

### 3.3 Results

A pyroclastic glass should have intra-sample chemical homogeneity. If a sample is truly homogeneous, any chemical variations will be solely due to analytical uncertainties. That is, if a glass displays intra-sample homogeneity, the standard deviation of individual EMP points should be less than the average uncertainty of the microprobe measurements. A homogeneous glass is one without quench phases or any other textural feature and that has a standard deviation which is less than the microprobe uncertainty for the non-volatile elements (Ti, Al, Cr, Fe, Mn, Mg, and Ca). Table 3 shows an example of the data for one of these glasses in sample QUE 94200,16. The standard deviation is also listed, but relative standard deviation is a more useful representation of the intra-sample heterogeneity of this glass since it factors out the difference in abundances between elements. A high relative standard deviation implies a large degree of heterogeneity. In terms of comparing the standard deviation of the analyses to the uncertainty of the microprobe, all elements show a greater standard deviation than microprobe uncertainties, meaning these variations cannot be explained by analytical uncertainties and, consequently, are real. Fig. 4 graphically displays the intra-sample heterogeneity of 4 glasses. The crosses represent the average microprobe uncertainty (they have different sizes because the scales in the figures differ), while the data points are actual analyses of glasses. The glasses depicted in (a), (b), and (c) are the most chemically homogeneous glasses involved in this study, while the glass in (d) displayed the most pristine texture of all the clasts. The fact that the data show greater variance than the microprobe uncertainty means that these glasses are not homogeneous for the elements involved in these plots (i.e., Mg and Fe). ***Of the 13 glasses analyzed, none of those without quench phases were chemically homogeneous for all the non-volatile elements listed.*** Using the essential criteria of intra-sample homogeneity, none of the glasses without quench phases appear to be pyroclastic glasses. Those with quench phases display textures (see Table 2) consistent with being impact-melt clasts (Fig. 5). Consequently, this study yielded no positive identification of pyroclastic glasses.

**Table 3.** Intra-sample heterogeneity of the non-volatile elements (wt %) of glass 15 in sample QUE 94200,16. Notice the variation in wt % of Cr and Ca in particular from analysis to analysis. For all elements, SD > uncertainty which means the glass is heterogeneous.

| **Analysis** | **$TiO_2$** | **$Al_2O_3$** | **$Cr_2O_3$** | **MgO** | **CaO** | **MnO** | **FeO** |
|---|---|---|---|---|---|---|---|
| 15i | 0.95 | 11.97 | 1.04 | 12.54 | 13.81 | 0.38 | 11.12 |
| 15ii | 0.74 | 12.46 | 0.35 | 12.51 | 14.14 | 0.37 | 10.63 |
| 15iii | 0.71 | 12.35 | 0.87 | 12.89 | 13.22 | 0.40 | 11.33 |
| 15iv | 0.74 | 12.58 | 0.25 | 12.98 | 13.09 | 0.34 | 11.22 |
| 15v | 0.59 | 12.51 | 0.18 | 13.04 | 12.73 | 0.37 | 11.33 |
| 15vi | 0.64 | 12.63 | 0.16 | 13.23 | 12.04 | 0.38 | 11.88 |
| 15vii | 0.61 | 12.76 | 0.14 | 13.75 | 10.31 | 0.40 | 12.88 |
| 15viii | 0.81 | 12.20 | 0.61 | 12.87 | 13.38 | 0.37 | 11.24 |
| 15ix | 0.71 | 12.43 | 0.45 | 12.89 | 12.68 | 0.34 | 11.33 |
| 15x | 0.74 | 12.61 | 0.12 | 13.03 | 11.78 | 0.36 | 11.72 |
| std dev (SD) | 0.10 | 0.23 | 0.33 | 0.35 | 1.11 | 0.02 | 0.60 |
| uncertainty | 0.098 | 0.158 | 0.063 | 0.194 | 0.415 | 0.048 | 0.285 |
| rel. SD (%) | 14.39 | 1.85 | 77.96 | 2.70 | 8.76 | 5.60 | 5.22 |

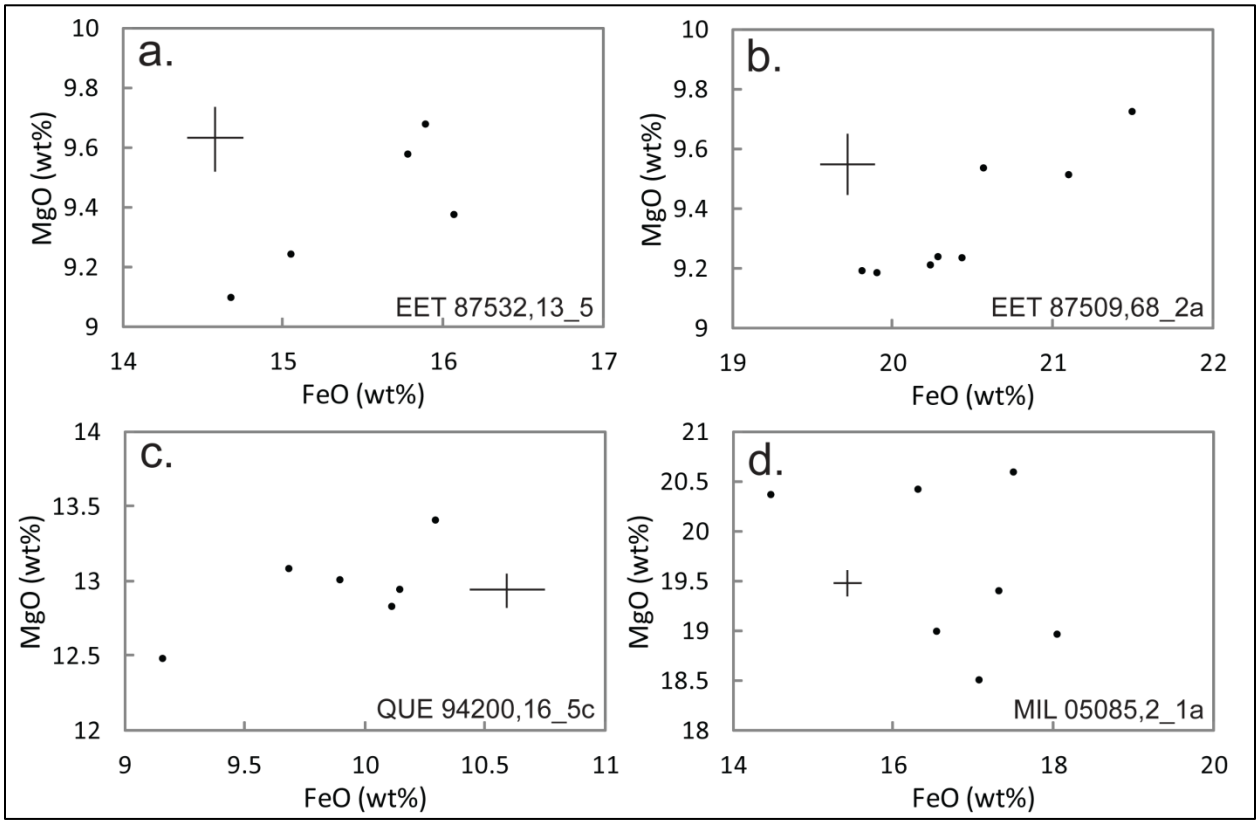


**Figure 4**. Variation diagrams illustrating the intra-sample heterogeneity of 4 glasses. The crosses represent the microprobe uncertainty. If the actual analyses of the glasses show more spread than the microprobe uncertainty, then they are heterogeneous.

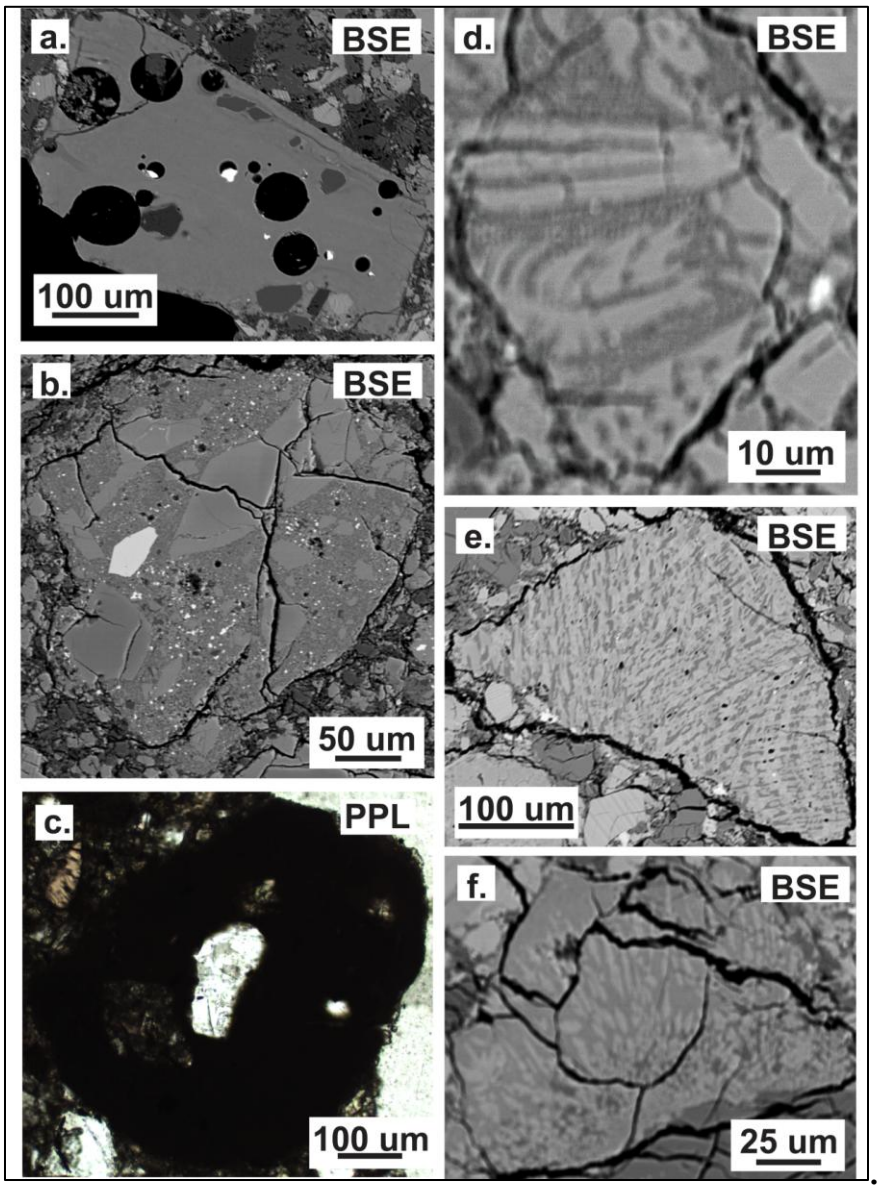


**Figure 5.** Howardite glasses with quench phases displaying textures consistent with an impact melt origin. (a) from MIL 05085,11; (b) from EET 87532,13; (c) from LAP 04838,19; (d) from EET 87509,68; (e) from LAP 04838,19; and (f) from EET 87509,68.

### 3.4 Discussion

The failure to identify any pyroclastic glasses in the howardite samples analyzed in this study may imply that pyroclastic glasses did not form on Vesta. There are a number of possible explanations for why pyroclastic material may not have been found in the howardites and, by extension, on Vesta.

(1) *Pyroclastic glasses exist on Vesta but were not present in the 8 howardites analyzed*. Given the number of glasses analyzed and the fact that the howardites studied were chosen to maximize the possibility of finding unusual glasses, this explanation is not the most realistic.

(2) *Pyroclastic glasses formed but were not retained on the surface*. This scenario would only occur if all pyroclastic material, regardless of size, was ejected from Vesta with a velocity greater than or equal to the Vestan escape velocity (~390 m/s). For this speed to be achieved, the erupting magma would have needed a gas content of at least 6 % by mass (Wilson and Keil, 1991; 1997; Wilson et al., 2010). In reality, ejecta have a range of speeds, so even at the highest gas contents we would expect some material to have ejection velocities less than the escape velocity. This explanation is also unlikely due to the extremely high volatile contents required, especially since Vesta is believed to be volatile-poor (e.g., Mittlefehldt, 1987; Grady et al., 1997a & b).

(3) *Pyroclastic glasses exist on Vesta but were covered by blankets of ejecta*. Vesta has been largely resurfaced by several massive impacts such as those that created the Veneneia and Rheasilvia basins at the South Pole (Schenk et al., 2012). The relatively young formation ages of Veneneia at ~2.1 Ga and Rheasilvia at ~1.0 Ga (Marchi et al., 2012), relative to the ancient ages of Vestan magmatism inferred from radiometric ages of HEDs (e.g., McSween et al., 2011), makes this mechanism plausible. Still, researchers expect that most HEDs were liberated from Vesta by one of these massive impact events. If they were ejected as a result of the Rheasilvia impact, then any consequent resurfacing from that impact would not affect the HED meteorites, and therefore, not explain the absence of pyroclastic glasses. Only an impact event (e.g., Veneneia) preceding Rheasilvia's formation could cause the resurfacing necessary to bury pyroclastic deposits under blankets of ejecta. An additional factor in this line of reasoning involves the depth of ejecta from the initial impact and the excavation depth from Rheasilvia. The blanket of ejecta that hypothetically buried pyroclastic material would need to be deeper than the excavation depth, otherwise the buried pyroclastic glasses would have been ejected from Vesta and be present in the HED collection. The Rheasilvia impact reached lower crustal/upper mantle levels as evidenced by the presence of exposed diogenite material at the Vestan South Pole (De Sanctis et al., 2012), and it is highly unlikely that pyroclastic material could have been buried to these depths.

(4) *Pyroclastic glasses formed but were thermally metamorphosed.* It is possible that fire-fountaining occurred on Vesta with all the necessary conditions to form discrete pyroclastic glasses, which were subsequently thermally metamorphosed causing them to recrystallize and appear texturally similar to impact-melt clasts. Most eucrites have experienced thermal metamorphism (Nyquist et al., 1986; Takeda and Graham, 1991; Bogard et al., 1993; Yamaguchi et al., 1994). However, due to the possibility of concurrent magmatism (forming the pyroclastic glasses) and thermal metamorphism from impacts or blanketing of lava flows (McSween et al., 2010), we might still expect to see some pristine pyroclasts. In addition, any thermal metamorphism would not explain the large degrees of intra-sample heterogeneity observed in glasses without crystalline phases.

(5) *Pyroclastic glasses never erupted*. This would occur if the conditions necessary for the formation of fire-fountaining were not met, and so lava was never erupted explosively. The volatile inventory of Vesta is thought to be very low (Drake et al., 1989; Papike, 1998), but there is evidence for at least some magmatic volatiles in eucrites in the form of OH-bearing apatites (Sarafian et al., 2012) though these could have formed from processes unrelated to original volatile-contents in the Vestan mantle (i.e., fractional crystallization).

(6) *Pyroclastic glasses never formed*. If optically dense fire-fountains ejected material that did not cool quickly enough to form pyroclastic glasses, it could instead have accumulated in lava ponds and lakes (Wilson and Keil, 1997; Keil, 2002; Wilson et al., 2010). Over 99 % of the material ejected from an optically dense fire fountain on Vesta would be molten upon landing on the surface (Wilson and Keil, 1997) explaining the absence of pyroclastic glasses in howardites. A low volatile-content leads to optically dense fountains (Wilson and Keil, 1997), and Vesta is a volatile-poor body. This explanation does not contradict any existing information pertaining to Vesta, making it one of the more realistic approaches.

Of the six explanations presented, the most plausible scenarios are 5 and 6. It is difficult to rule out either of these options based on our existing understanding of Vesta.

## 4. GLASS GROUPS

Previous work delineating compositional glass groupings in howardites is limited. Barrat et al. (2012) identified two main glass groups: low Fe/Mg (FeO/MgO<5) and high Fe/Mg (FeO/MgO >>10). The 152 howardite glass analyses in the current study all had FeO/MgO < 5. Barrat et al. (2012) further divided the low Fe/Mg group into three subgroups: (1) low-alkali, (2) K-rich ($K_2O$ > 0.2 wt%), and (3) Na-rich ($Na_2O$ > 0.6 wt%). No Na-rich glasses were found in the current study, but an additional group, called Ca-rich, was identified. Of the 152 glass analyses in this study, 61 are K-rich, 16 are low-alkali, and 90 are Ca-rich.

### 4.1 Results

Variation diagrams illustrate the compositional differences between these glass groups. Figs. 6 and 7 show examples of such plots. Data were also obtained on the Na, Ti, and Cr abundances for these glasses, but these elements did not show any patterns or trends between groups. As noted by Barrat et al. (2012), the bulk compositions of the HEDs, represented by gray envelopes in Figs. 6 and 7, can only describe the bulk composition of the low-alkali glasses.

The Ca-rich glasses are labeled as such since all the outliers are enriched in CaO in comparison to HED values, although a particular cut-off value cannot be assigned to this group as Barrat et al. (2012) did for the K- and Na-rich groups (Fig. 7). This is due to the fact that while Na and K are present in low amounts (nearly detection limits) in the low-alkali glasses, Ca is abundant in all glass groups. The Ca-enrichment for the Ca-rich glasses is also accompanied by Al- and Si-enrichments relative to HEDs (Figs. 6a & d). Perplexing splotchy textures were noted for 5 of these Ca-rich impact melt clasts (Fig. 8). They appear to occur near the edges of the glass grains and are bright in backscatter, which may indicate that they are enriched in Fe. This would be consistent with an apparent Fe-depletion in the non-splotchy portions of the glasses indicating migration of Fe. The K-rich glasses also do not fall within the HED envelope but only with regard to K (Fig 6b). They agree with compositions found in other studies as the K-rich envelope of Barrat et al. (2009a) shows. This failure to plot within HED literature envelopes

means that these Ca-rich and K-rich glasses must have unique origins (e.g., different than typical impact melts from HED lithologies).

It is useful to see whether the REEs and other trace elements show similar patterns within a given group. Fig. 9 displays spider diagrams of trace elements for two of the three glass groups. The only glasses analyzed for trace elements belong to either the Ca-rich or K-rich groups because microprobe analyses were performed after the trace element data was obtained. Glasses within a given group show consistencies, but with the exception of Rb, K, and Na, the two groups shows similar patterns (e.g., REEs and Ni are enriched and Co is depleted); consequently, the major and minor elements are the distinguishing features for each glass group.

It is worthwhile to ask whether classification of glasses into distinct compositional groups is a useful or even valid investigational technique. For example, this technique only works for glasses without crystalline phases. A further complication arises when a single vitric clast contains different compositional groupings. Fig. 10 shows an example of a single glass containing multiple compositional domains. The chemically distinct portion is indicated with a white arrow. It is only apparent in plane-polarized light and in the Ca, K, and Na X-ray maps. The presence of multiple glass groups within a single seemingly crystal-free clast could be a common occurrence that goes unnoticed if analyses from a glass are averaged. It is not the existence of compositionally distinct glasses in the HED suite that is being called into question but rather the means that researchers use to analyze these glasses. This is further support for the technique used in this study in which we treated every analysis separately rather than averaging all analyses from a glass.

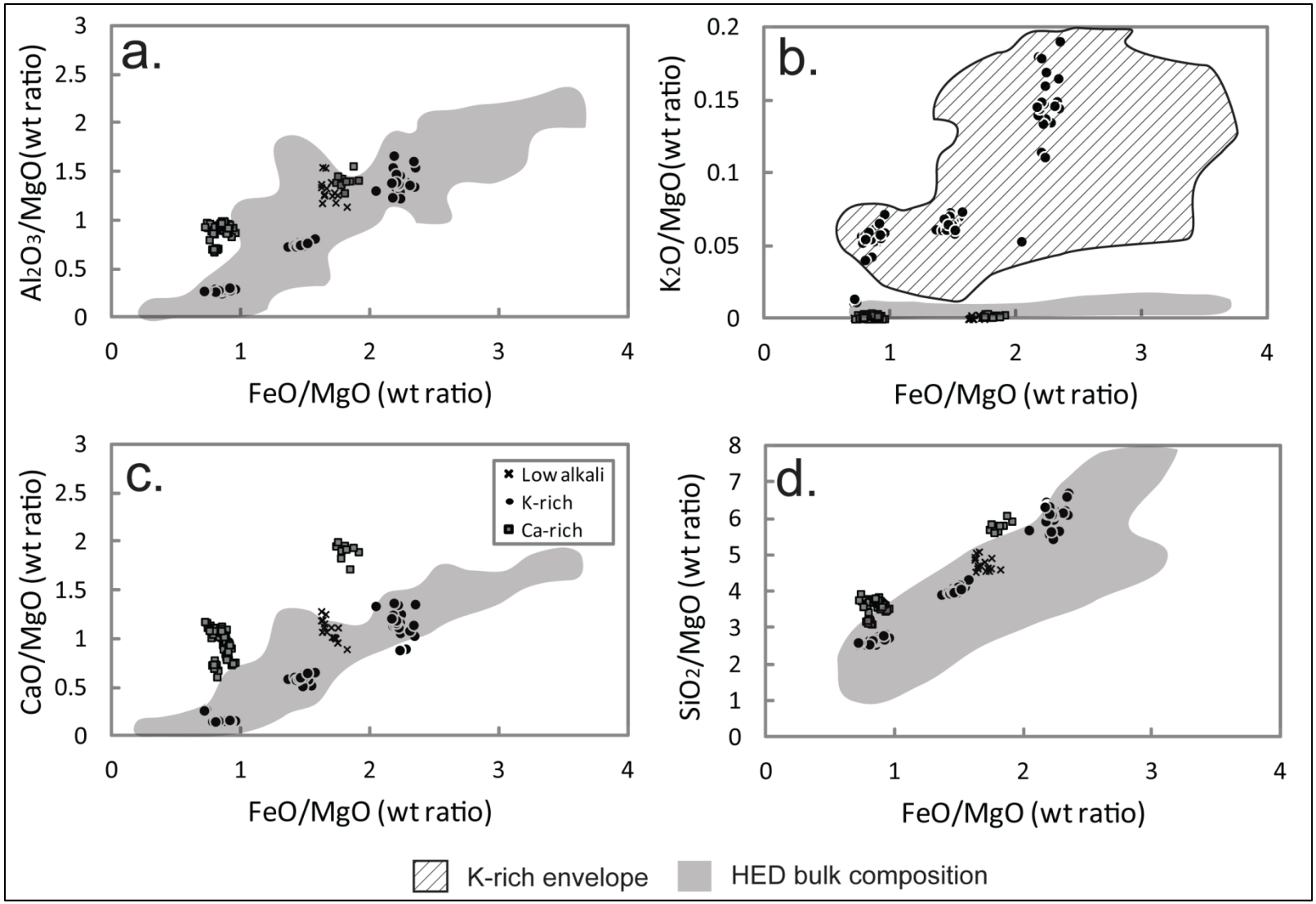


**Figure 6.** Variation diagrams of the 152 howardite glass analyses. Note that the K-rich glasses fall outside of the HED envelope but within the K-rich envelope in (b), while the Ca-rich glasses fall outside the HED envelope in (a), (c), and (d). Literature data from Usui et al. (2010) and references therein, Warren et al. (2009b), and Barrat et al. (2009a).

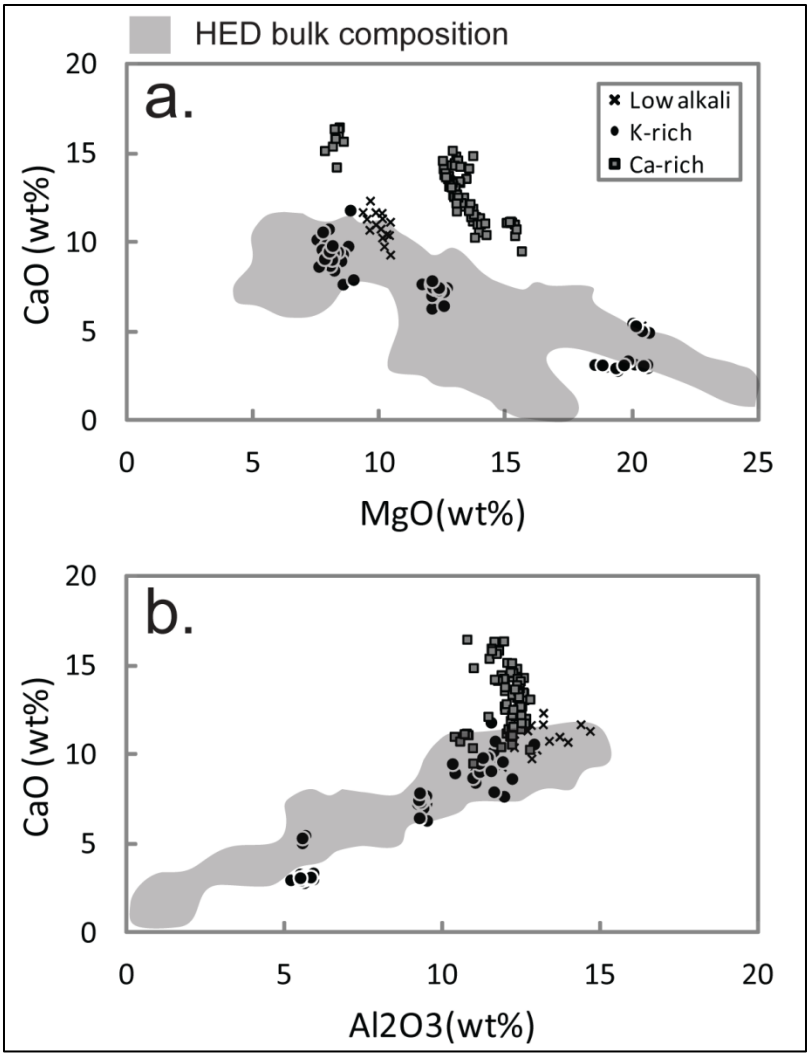


**Figure 7.** Additional variation diagrams of howardite glass groups focusing on the behavior of the Ca-rich glasses. Notice that the Ca-rich glasses consistently plot outside of the HED envelope in terms of Ca. Literature data from Usui et al. (2010) and references therein and Warren et al. (2009b).

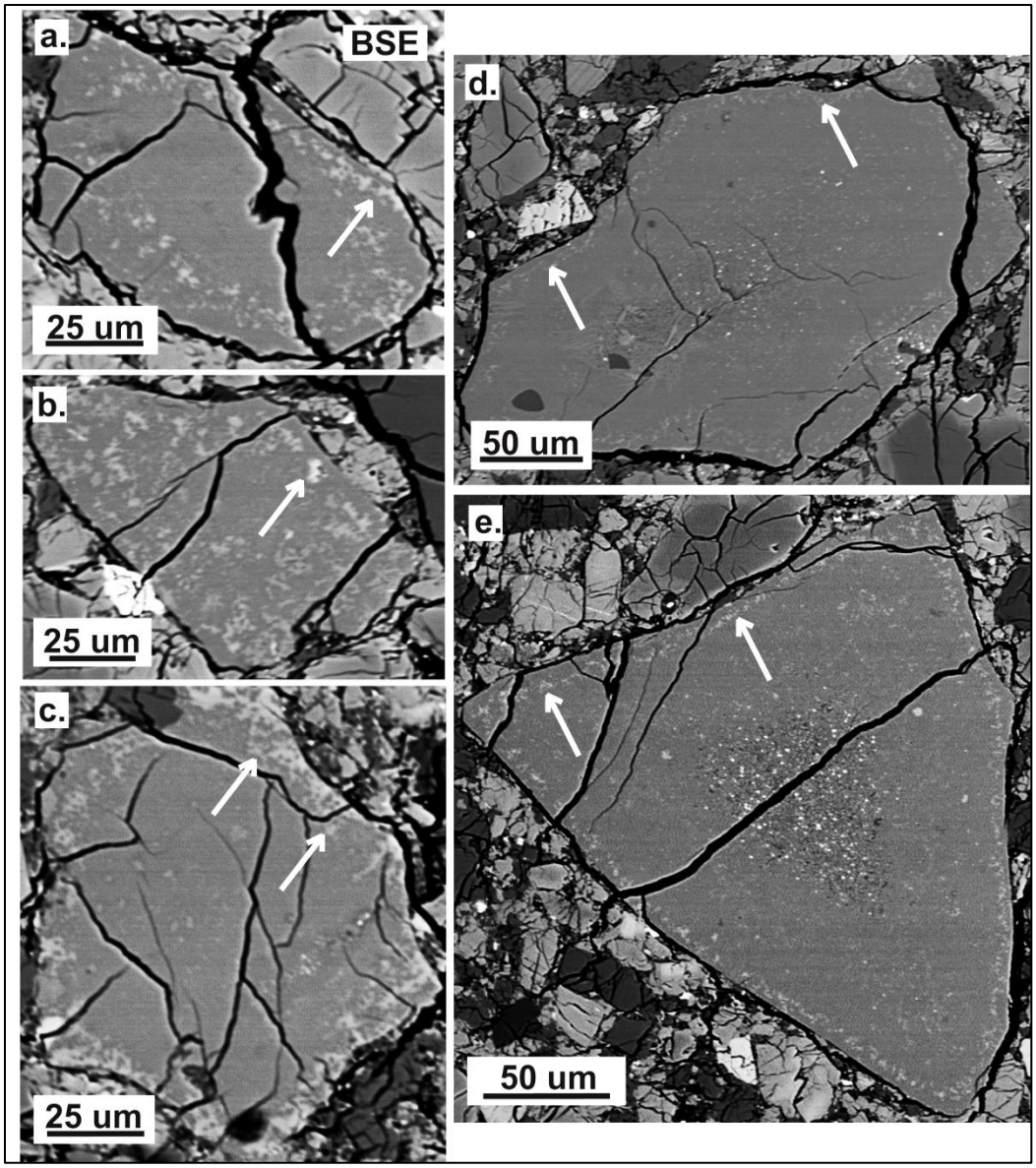


**Figure 8.** Perplexing splotchy textures seen in 5 of the Ca-rich glasses. This splotchy texture appears concentrated near the edges of the grains. All glasses from QUE 94200,16.

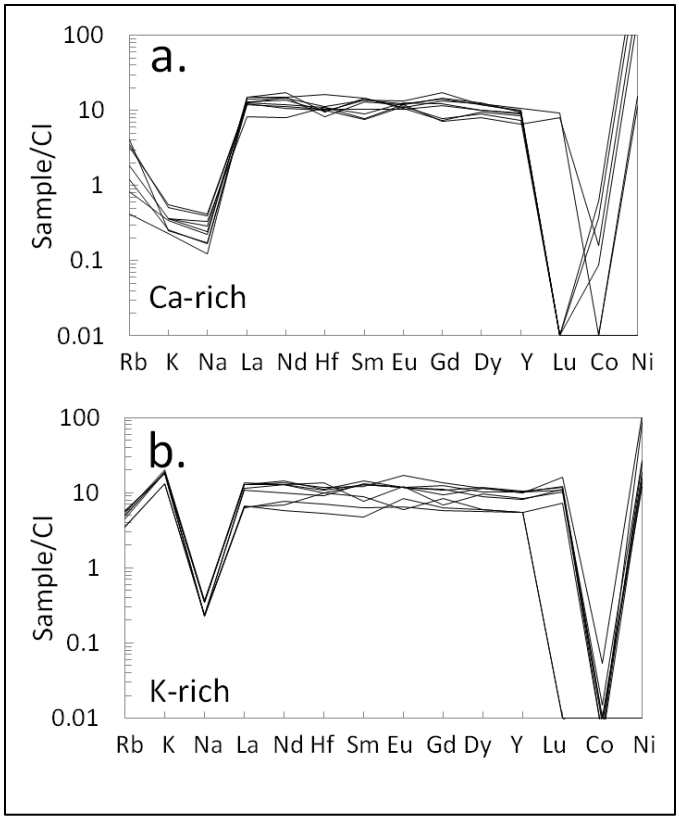


**Figure 9.** Trace-element spider diagrams of the (a) Ca-rich, and (b) K-rich howardite glass groups. Note the patterns only differ in terms of Rb, K, and Na. CI data from Anders and Grevesse (1989).

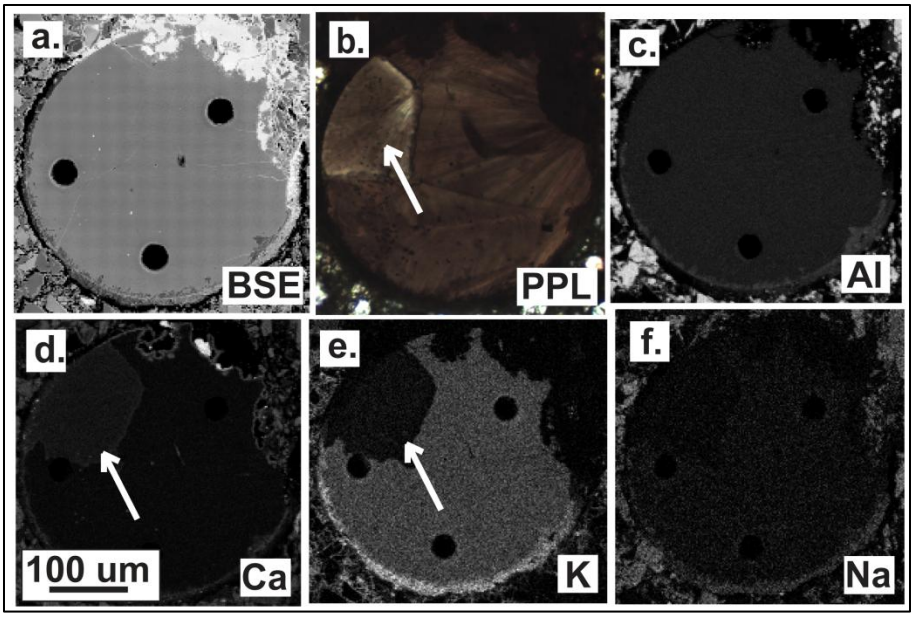


**Figure 10.** Backscattered electron (a), plane-polarized light (b), and X-ray map images (c)-(f) of glass 1a in sample MIL 05085,2. The presence of a compositionally distinct portion of the glass is obvious in (b), (d), and (e) and is designated by the white arrows.

## 4.2 Discussion

The discovery of K-rich and Ca-rich glasses in this study is particularly interesting. Previous authors such as Barrat et al. (2009a, 2009b) and Warren et al. (2009b) have identified and characterized members of the K-rich group. The glasses range in shape from spheres to angular fragments and in texture from vitric to vesicular to crystal-rich. The Ca-rich glasses, on the other hand, have not been previously identified in howardites.

It is worthwhile to ask whether the K-rich glasses could be pyroclastic in origin. Some exhibit shapes, textures, and chemical features (i.e., enrichment in volatile elements such as K) consistent with this. Still, there are factors that strongly imply a non-pyroclastic genesis such as the absence of alkali-element coatings on the spherical glasses as seen in lunar volcanic glasses (Meyer et al., 1975; Barrat et al., 2009b), and the presence of Fe-Ni metal and troilite grains or dust (Barrat et al., 2009a). Also, the enrichments in K are so extreme as to suggest that these glasses could not have formed from any previously recognized lithology on Vesta as seen in the HEDs (Barrat et al., 2009b). Chemical similarities among any group of glasses, even with vastly differing textures, indicate a common source (Hewins and Klein, 1978). K-rich glasses seen in howardites share such compositional similarities, and so it is more logical to suspect that each group might derive from impacts onto a shared heterogeneous lithology rather than being pyroclastic glasses that were erupted from the same magma source.

The chemical characteristics of the K-rich glasses point to a non-HED composition of their protolith. It is important to note that the bulk compositions of impact melts are not necessarily equivalent to the original composition of the material impacted, especially in small impacts (Reid et al., 1972). This is largely due to fractionations that occur as a result of glass formation and mostly affects the alkali elements (Gibson and Hubbard, 1972). Still, the K-enrichments seen here are rather extreme. Felsic compositions are a rarity on planetary bodies other than Earth, but they do exist as small, localized samples such as the lunar "granites" (e.g., Drake et al., 1970; Meyer, 1972; Ryder et al., 1975; Glass 1976).

A possible scenario for the formation of K-rich melts on Vesta involves a global magma ocean producing KREEP-like melts much like what we see on the Moon. KREEP melts form from the highly fractionated last dregs of a global magma ocean (e.g., Meyer, 1977; Warren and Wasson, 1979b; Warren, 1989). Lunar KREEP components usually occur in brecciated samples much like the K-rich glasses occurring in howardites (Papike et al., 1998). This scenario is unlikely since the K-rich glasses do not show REE-enrichments in comparison to basaltic eucrite compositions, and there is still debate on whether Vesta had a global magma ocean (e.g., Ikeda and Takeda, 1985; Righter and Drake 1997; Ruzicka et al., 1997; Takeda, 1997; Warren, 1997; Greenwood et al., 2005; Barrat et al., 2008). But in cases of extreme fractional crystallization, the K-portion of the KREEP melt can separate from the REEP-portion through liquid immiscibility. It is has been experimentally shown by Powell et al. (1980) that eucritic liquids can produce K-rich compositions through liquid immiscibility. This may be the mechanism that generated the K-rich glasses in howardites, although the silica contents of the glasses are not especially high (~50 wt %). Also, the REEP-melt (Fe-rich) that should be complimentary to the K-melt (K- and Si-rich) has not yet been indentified in any HED sample. Instead, these glasses may be the result of impact onto a feldspar-rich lithology formed by partial melting of the eucritic crust (J. A. Barrat, personal communication).

The origin of the Ca-rich glasses is less conjectural since there are not extreme enrichments of alkali elements. In terms of all elements but Ca, Al and Si, these glasses are

similar to HED bulk compositions. Since Ca-enrichments are usually associated with Al- and Si-enrichments, these glasses likely represent impact onto HED lithologies with a preferential melting of plagioclase. This explanation is reasonable since feldspars are the first phase to melt from shock metamorphism (Schaal et al., 1979; Stoffler et al., 1991). Strangely, a positive Eu anomaly is not seen with these Ca-rich glasses (Fig. 9a) as would be expected for plagioclase-derived melts.

## 5. CONCLUSIONS

This work characterizes the textures and compositions of 56 glasses in 8 howardites using petrography and electron microprobe and LA-ICP-MS analyses. Impact-melt clasts and pyroclastic glasses from lunar samples were used to determine textural and compositional differences between the two glass types. Distinct chemical differences between the two types were found, but not all the lunar criteria are useful for Vestan samples due to distinct differences between the two bodies. Glass groupings reported in other work (Barrat et al., 2012) were explored for the glasses of this study. A summary of the more significant findings of this study are listed below:

- The Vestan criteria yielded no positive identification of putative pyroclastic glasses.
- Six explanations for the absence of pyroclastic material in the HEDs were considered. The most plausible are that (1) pyroclastic eruptions did not occur because of low volatile contents in magmas, or (2) optically dense fire-fountaining prevented the formation of pyroclastic deposits.
- The analyzed howardite glasses can be divided into 3 groups based on composition: K-rich, Ca-rich, and low-alkali. The K-rich and Ca-rich groups plot outside the range of known HEDs. Previous work identified the K-rich and low-alkali glasses, whereas this work is the first to identify the Ca-rich glasses.
- The K-rich glasses are likely the result of impacts onto previously unrecognized feldspar-rich lithologies, perhaps originating from partial melting of crustal material.
- The low-alkali and Ca-rich glasses represent impact onto HED lithologies, but the Ca-rich have characteristics indicative of preferential melting of plagioclase.

## References


Anders E. and Grevesse N. 1989. Abundances of the elements: Meteoritic and solar. *Geochimica et Cosmochimica Acta* 53:197-214.

Barrat J. A., Yamaguchi A, Greenwood R. C., Benoit M., Cotton J., Bohn M., and Franchi I. A. 2008. Geochemistry of diogenites: Still more diversity in their parental melts. *Meteoritics & Planetary Science* 43(11):1759-1775.

Barrat J. A, Bohn, M., Gillet PH., Yamaguchi A. 2009a. Evidence for K-rich terranes on Vesta from impact spherules. *Meteoritics & Planetary Science* 44:359-374.

Barrat J. A, Yamaguchi A., Greenwood R. C., and Bollinger C. 2009b. Trace element geochemistry of K-rich impact spherules from howardites. *Geochimica et Cosmochimica Acta* 73:5944-5958.

Barrat J. A., Bodenan J. D., Yamaguchi A., Buchanan P. C., Toplis M., and Bollinger C. 2012. What can we learn on Vesta from the petrology of impact melts? (abstract). *Lunar Planetary Science* 43:1438.

Beck A. W., Mittlefehldt D. W., McSween H. Y., Rumble D., Lee C.-T. A., and Bodnar R. J. 2011. MIL 03443, a dunite from Asteroid 4 Vesta: Evidence for its classification and cumulate origin. *Meteoritics & Planetary Science* 46:1133-1151.

Bell J. F. et al. 2002. Near-IR reflectance spectroscopy of 433Eros from the NIS instrument on the NEAR mission. *Icarus* 155:119-144.

Bogard, D. D., Nyquist L., Takeda H., Mori, H., Aoyama T., Bansal B., Wiesman H., and Shih C. Y. 1993. Antarctic polymict eucrite Yamato 792769 and the cratering record on the HED parent body. *Geochimica et Cosmochimica Acta* 57:2111-2121.

Brunfelt A.O., Heier K.S., Nilssen B., Steiennes E., and Sundvoll B. 1972. Elemental composition of Apollo 15 samples. In: Chamberlain J.W. and Watkins C., editors. The Apollo 15 Lunar Samples, 195-197. Lunar Science Institute, Houston

Butler P. Jr. 1978. Recognition of lunar glass droplets produced directly from endogenous liquids: The evidence from S-Zn coatings. *Proc. Lunar Planetary Science Conference* 9:1459-1471.

Caffee M. W., Goswami J. N., Hohenburg C. M., Marti K., and Reedy R. C. 1988. In: Kerridge J. F. and Matthews M.S., editors. *Meteorites and the Early Solar System*. Tuscon: Univ. of Arizona Press. pp. 205.

Chapmann C. R. 1997. S-type asteroids, ordinary chondrites, and space weathering: The evidence from Galileo's flybys of Gaspra and Ida. *Meteoritics & Planetary Science* 31:699-725.

Chou C. L., Boynton W. V., Sundberg L. L., Wasson J. T. 1975. Volatiles on the surface of Apollo 15 green glass and trace-element distributions among Apollo 15 soils. *Proc. Lunar Planetary Science Conference* 6:1701-1727.

Delano J. W. 1986. Pristine lunar glasses: Criteria, data, and implications. *Journal of Geophysical Research* 91(B4):D201–D213

Delano J. W. 1991. Geochemical comparison of impact glasses from lunar meteorites ALHA and MAC88105 and Apollo 16 regolith 64001. *Geochimica et Cosmochimica Acta* 55:3019-3029.

Delano J. W., Lindsley D. H., and Rucowski R. 1981. Glasses of impact origin from Apollo 11, 12, 15, and 16: Evidence for fractional vaporization and mare/highland mixing. *Proc. Lunar Planetary Science Conference* 12:339-370.

De Sanctis M. C. et al. 2012. Spectroscopic characterization of mineralogy and its diversity across Vesta. *Science* 336:697-700.

Dohnanji J. S. 1975. Sources of interplanetary dust: Asteroids. In: Elsaesser H. and Fechtig H., editors. *Interplanetary Dust and Zodiacal Light*. New York: Springer Verlag, pp. 187-205.

Drake M. J., McCallum I. S., McKay G. A., and Weill D. F. 1970. Mineralogy and petrology of Apollo 12 sample no. 12013: A progress report. *Earth Planetary Science Letters* 9:103-123.

Drake M. J., Newson H. E., Capobianco C. J. 1989. V, Cr, and Mn in the Earth, Moon, EPB and SPB and the origin of the Moon: Experimental studies. *Geochimica et Cosmochimica Acta* 53:2101-2111.

Fudali R. F., Kreutzberger M., Kurat G., and Brandstatter F. 1984. Aspects of a glassy meteorite from the Moon bearing on some problems in extraterrestrial glass-making. *Journal of Non-Crystalline Solids* 67:383-396.

Gast P. W. 1968. Trace element fractionation and the origin of tholeiitic and alkaline magma types. *Geochimica et Cosmochimica Acta* 32:1057-1086

Gibson E. K. and Hubbard N. J. 1972. Volatile element depletion investigations on Apollo 11 and 12 lunar basalts via thermal volatilization. In: Watkins C., editor. *Lunar Science* III, Lunar Science Institute Contr. No. 88. pp. 303-305.

Glass B. P. 1976. High-silica lunar glasses in an Apollo 14 soil sample: Evidence for silicic lunar volcanism? *Earth Planetary Science Letters* 33:79-85.

Grady M. M., Wright I. P., and Pillinger C. T. 1997. Indigenous primitive carbon in eucrites and diogenites (abstract). *Lunar Planetary Science* 28:443-444.

Grady M. M., Wright I. P., and Pillinger C. T. 1997. Carbon in howardite, eucrite and diogenite basaltic achondrites. *Meteoritics & Planetary Science* 32:863-868.

Greenwood R. C., Franchi I. A., Jambon A. ,and Buchanan P. C. 2005. Widespread magma oceans on asteroidal bodies in the early solar system. *Nature* 435:916-918.

Grun E., Fechtig H., Kissel J., and Gammelin P. 1977. Micrometeoroid data from the first two orbits of Helios 1. *Journal of Geophysical Research* 42:717-726.

Hartmann W. K. 1977. Relative crater production rates on planets. *Icarus* 31:260-276.

Heiken G. H. and McKay D. S. 1974. Lunar deposits of possible pyroclastic origin. *Geochimica et Cosmochimica Acta* 38:1703-1718.

Hewins R. H. and Klein L. C. 1978. Provenance of metal and melt rock textures in the Malvern howardite. *Proc. Lunar and Planetary Science Conference* 9:1137-1156.

Horz F., Cintala M. J., See T. H., and Loan L. E. 2005. Shock melting of ordinary chondrite powders and implications for asteroidal regoliths. *Meteoritics & Planetary Science* 40:1329-1346.

Ikeda Y. and Takeda H. 1985. A model for the origin of basaltic achondrites based on the Yamato-7308 howardite. Proceedings,15th Lunar and Planetary Science Conference. *Journal of Geophysical Research* 90:C649–C663.

Ivanov A. V. and Florensky K. P. 1975. The role of vaporization process in lunar rock formation. *Proc. Lunar Planetary Science Conference* 6:1341-1350.

Jeanloz R. F. and Ahrens T. J. 1976. Alkali mobility in shocked basalt. In: Watkins C., editor. *Lunar Science* VII. Houston: Lunar Science Institute. pp.428-430.

Keil K. 2002. Geological history of asteroid 4 Vesta: the "smallest terrestrial planet". In: W. Bottke, A. Cellino, P. Paolicchi, and R. Binzel, editors. *Asteroids III*. Tuscon: Arizona LPI Publishing, pp. 573-585.

Keil K., Stoffler D., Love S. G., and Scott E. R. D. 1997. Constraints on the role of impact heating and melting on asteroids. *Meteoritics & Planetary Science* 32:349-363.

Keller L. P. and McKay D. S. 1991. Analytical electron microscopy of fine-grained glass spheres in Apollo 16 soil 61181 (abstract). *Lunar Planetary Science XXII*, pp. 703-704.

Keller L. P. and McKay D. S. 1992. Micrometer-sized glass spheres in Apollo 16 soil 61181: Implications for impact volatilization and condensation. *Proc. Lunar Planetary Science Conference* 22:137-141.

Labotka T. C and Papike J. J. 1980. Howardites: samples of the regolith of the eucrite parent-body: petrology of Frankfort, Pavlovka, Yurtuk, Malvern, and ALHA 77302. *Proc. Lunar Planetary Science Conference* 11:1103-1130.

Langenhorst F. 2002. Shock metamorphism of some minerals: Basic introduction and microstructural observations. *Bulletin of the Czech Geological Survey* 77:265-282.

Laul J. C., Simon S. B., and Papike J. J. 1988. Chemistry and petrology of the Apennine Front, Apollo 15, Part II: Impact melt rocks. *Proc. Lunar Planetary Science* 18:203-217.

Ma M. S., Liu Y. G., and Schmitt R. A. 1981. A chemical study of individual green glasses and brown glasses from 15426: Implications for their petrogenesis. *Proc. Lunar Planetary Science* 12B:915-933

Marchi S., McSween H. Y., O'Brien D. P., Schenk P., De Sanctis M. C., Gaskell R., Jaumann R., Mottola S., Preusker F., Raymond C. A., Roatsch T., Russell C. T. 2012. The violent collisional history of asteroid 4 Vesta. *Science*, in press.

McSween H. Y., Mittlefehldt D. W., Beck A. W., Mayne R. G., and McCoy T. J. 2011. HED meteorites and their relationship to the geology of Vesta and the Dawn mission. *Space Science Reviews* 163:141-174, doi:10.1007/s11214-010-9637-z.

Melosh H. J. and Vickery A. M. 1991. Melt droplet formation in energetic impact events. *Nature* 350:494-497.

Meyer Jr. C. 1972. Mineral assemblages and the origin of non-mare lunar rock types (abstract). *Lunar Science* 3:542-544.

Meyer Jr. C. 1977. Petrology, mineralogy, and chemistry of KREEP basalt. *Physics and Chemistry of the Earth* 10:239-260.

Meyer Jr. C., McKay D. S., Anderson D. H., and Butler Jr. P. 1975. The source of sublimates on the Apollo 15 green and Apollo 17 orange glass samples. *Proc. Lunar Planetary Science Conference* 6:1673–1699.

Mittlefehldt D. W. 1987. Volatile degassing of basaltic achondrite parent bodies: Evidence from alkali elements and phosphorus. *Geochimica et Cosmochimica Acta* 51:267-278.

Mittlefehldt D. W. and Lindstrom M. M. 1997. Magnesian basalt clasts from the EET 92014 and Kapoeta howardites and a discussion of alleged primary magnesian HED basalts. *Geochimica et Cosmochimica Acta* 61:453-462.

Mittlefehldt D. W., McCoy T. J., Goodrich C. A., and Kracher A. 1998. Non-chondritic meteorites from asteroidal bodies. In: Papike J. J., editor. *Planetary Materials. Reviews in Mineralogy*, vol. 36, chapter 4. Min. Soc. Am., pp. 1-195.

Mutchler S. T., Fedele L., and Bodnar R. J. 2008. Analysis Management System (AMS) for reduction of laser ablation ICP-MS data. In: Sylvester P., editor. *Montreal Laser ablation ICP-MS in the earth sciences: Current practices and outstanding issues.* Mineralogical Association of Canada. Short Course 40. pp. 503–353.

Naney M. T., Crowl D. M., and Papike J. J. 1976. The Apollo 16 drill core: Statistical analysis of glass chemistry and the characterization of a high alumina-silica poor (HASP) glass. *Proc. Lunar Planetary Science Conference* 7:155-184.

Norman M. D., Pearson N. J., Sharma A., and Griffin W. L. 1996. Quantitative analysis of trace elements in geological materials by laser ablation ICPMS: Instrumental operating conditions and calibration values of NIST glasses. *Geostandards Newslater* 20:247-261.

Nyquist L. E., Takeda H., Bansal B. M., Shih C. Y., Wiesmann H., and Wooden J. L. 1986. Rb-Sr and Sm-Nd internal isochron ages of a subophitic basalt clast and a matric sample from the Y75011 eucrite. *Journal of Geophyiscal Research* 91:8137-8150.

Papike J. J. 1998. Comparative planetary mineralogy: Chemistry of melt-derived pyroxene, feldspar, and olivine. In: Papike J. J., editor. *Planetary Materials. Reviews in Mineralogy*, vol. 36, chapter 7. Min. Soc. Am., pp. 1-11.

Papike J. J., Spilde M. N., Adcock C. T., Fowler G. W., and Shearer C. K. 1997. Trace element fractionation by impact-induced volatilization: SIMS study of lunar HASP samples. *American Mineralogist* 82:603-604.

Papike J. J, Ryder G., and Shearer C. K. 1998. Lunar samples. In: Papike J. J., editor. *Planetary Materials. Reviews in Mineralogy*, vol. 36, chapter 5. Min. Soc. Am., pp. 1-234.

Pierazzo E., Vickery A. M., and Melosh H. J. 1997. A reevaluation of impact melt production. *Icarus* 127:408-423.

Powell M. A., Walker D., and Hays J. F. 1980. Controlled cooling and crystallization of a eucrite: Microprobe studies. *Proc. Lunar Planetary Science Conference* 11:1153-1168.

Reid A. M., Warner J., Ridley W. I., Johnston D. A., and Harmon R. S. 1972. The major element compositions of lunar rocks as inferred from glass compositions in the lunar soil. *Proc. Lunar and Planetary Science Conference* 3:363-378.

Righter K. and Drake M. J. 1997. A magma ocean on Vesta: Core formation and petrogenesis of eucrites and diogenites. *Meteoritics & Planetary Science* 32:929-944.

Roedder E. and Weiblen P. W. 1973. Apollo 17 “orange soil” and meteorite impact on liquid lava. *Nature* 224:210-212.

Ruzicka A., Snyder G. A., and Taylor L. A. 1997. Vesta as the howardite, eucrite and diogenite parent body: Implications for the size of a core and for large-scale differentiation. *Meteoritics & Planetary Science* 32:825-840.

Ryder G. and Schuraytz B.C. 2001. Chemical variations of the large Apollo 15 olivine-normative mare basalt rock samples. *Journal of Geophysical Research* 106:1435-1451.

Ryder G. and Spudis P. 1987. Chemical composition and origin of Apollo 15 impact melts. *Journal of Geophysical Research* 92:E432-46.

Ryder G., Stoeser D. B., Marvin U. B., and Boyer J. F. 1975. Lunar granites with unique ternary feldspars. *Proc. Lunar Science Conference* 6:435-449.

Sarafian A. R., Roden M. F., and PatiñoDouce A. E. 2012. The nature of volatiles in Vesta: Clues from apatite in eucrites (abstract). *Lunar Planetary Science* 43:1175

Schaal R. B. and Horz F. 1977. Shock metamorphism of lunar and terrestrial basalts. *Proc. Lunar and Planetary Science Conference* 8:1697-1729.

Schaal R. B., Horz F., Thompson T. D., and Bauer J. F. 1979. Shock metamorphism of granulated lunar basalt. *Proc. Lunar and Planetary Science Conference* 10:2547-2571.

Schenk P. et al. 2012. The geologically recent giant impact basins at Vesta's south pole. *Science*, 336:694-697.

Schmid R. 1981. Descriptive nomenclature and classification of pyroclastic deposits and fragments: Recommendations of the IUGS subcommission on the systematics of igneous rocks. *Geology* 9:41-43.

Shearer C. K. and Papike J. J. 1993. Basaltic magmatism on the Moon: A perspective from volcanic picritic glass beads. *Geochimica et Cosmochimica Acta* 57:4785-4812.

Shearer C. K., Papike J. J., Simon S. B., Shimizu N., Yurimoto H., and Sueno S. 1990. Ion microprobe studies of trace elements in Apollo 14 volcanic glass beads: Comparisons to Apollo 14 mare basalts and petrogenesis of picritic magmas. *Geochimica et Cosmochimica Acta* 54:851-867.

Shearer C. K., Papike J. J., Galbreath K. C., Shimizu N. 1991. Exploring the lunar mantle with secondary ion mass spectrometry: A comparison of lunar picritic glass beads from the Apollo 14 and Apollo 17 sites. *Earth and Planetary Science Letters* 102:134-147.

Stoffler D., Keil K. and Scott E. R. D. 1991. Shock metamorphism of ordinary chondrites. *Geochimica et Cosmochimica Acta* 55:3845-3867.

Stolper E. 1977. Experimental petrology of eucritic meteorites. *Geochimica et Cosmochimica Acta* 41:587-611.

Stone C. D., Taylor L. A., McKay D. S., and Morris R. V. 1982. Ferromagnetic resonance intensity: A rapid method for determining lunar glass bead origin. *Journal of Geophysical Research* 87: A182-A196.

Takeda H. 1997. Mineralogical records of early planetary processes on the howardite, eucrite, diogenite parent body with reference to Vesta. *Meteoritics & Planetary Science* 32:841-853.

Takeda H and Graham A. L. 1991. Degree of equilibration of eucritic pyroxenes and thermal metamorphism of the earliest planetary crust. *Meteoritics* 26:129-134.

Taylor S. R., Taylor G. F., and Taylor L. A. 2006. The Moon: A Taylor perspective. *Geochimica et Cosmochimica Acta* 70:5904-5918.

Thomas P. C., Binzel R. P., Gaffey M. J., Storrs A. D., Wells E. N., and Zellner B. H. 1997. Impact excavation on Asteroid 4 Vesta: Hubble Space Telescope results. *Science* 277(5331):1492-1495.

Usui T., McSween H. Y. Jr., Mittlefehldt D. W., and Prettyman T. H. 2010. K-Th-Ti systematics and new three-component mixing model of HED meteorites: Prospective study for interpretation of gamma-ray and neutron spectra for the Dawn mission. *Meteoritics & Planetary Science* 45:1170-1190

Vaniman D. T. 1990. Glass variants and multiple HASP trends in Apollo 14 regolith breccias. *Proc. Lunar Planetary Science Conference* 20:209-217.

Vickery A. M. and Melosh H. J. 1991. Production of impact melt in craters on Venus, Earth, and the Moon. *Lunar Planetary Science* 22:1443-1444.

Warren P. H.1989. KREEP: Major-element diversity, trace element uniformity (almost) (abstract). In: Workshop on Moon in transition: Apollo 14, KREEP, and Evolved Lunar Rocks, LPI Tech Report 89-03, p 149-53, Lunar and Planetary Institute, Houston.

Warren P. H. 1997. Magnesium oxide-iron oxide mass balance constraints and a more detailed model for the relationship between eucrites and diogenites. *Meteoritics & Planetary Science* 32:945-963.

Warren P. H. and Wasson J. T. 1979. The origin of KREEP. *Reviews of Geophysics and Space Research* 17:73-88.

Warren P. H., Huber H., and Choe W. 2009a. Siderophile and other geochemical mixing relationships among HED-meteoritic breccias: Need for recognition of regolithic howardites as a distinctive subtype (abstract). *Lunar Planetary Science* 40:2471.

Warren P. H., Kallemeyn G. W., Huber H., Ulff-Moller F., and Choe W. 2009b. Siderophile and other geochemical constraints on mixing relationships among HED-meteoritic breccias. *Geochimica et Cosmochimica Acta* 73:5918-5943.

Wasson J. T., Boynton W. V., Kallemeyn G. W., Sundberg L. L., Wai C. M. 1976. Volatile compounds released during lunar lava fountaining. *Proc. Lunar Planetary Science Conference* 7:1583-1595.

Wilkening L. L. 1973. Foreign inclusions in stony meteorites – I. Carbonaceous chondrite xenoliths in the Kapoeta howardite. *Geochimica et Cosmochimica Acta* 37:1985-1989.

Wilson, L., and Head J. W. 1981. Ascent and eruption of basaltic magma on the earth and moon, *Journal of Geophysical. Research* 86(B4):2971-3001.

Wilson L. and Keil K. 1991. Consequences of explosive eruptions on small solar system bodies; The case of the missing basalts on the aubrite parent body. *Earth Planetary Science Letters* 104:505-512.

Wilson L. and Keil K. 1997. The fate of pyroclasts produced in explosive eruptions on the asteroid 4 Vesta. *Meteoritics & Planetary Science* 32(6):813-823.

Wilson L., Keil K., and McCoy T.J. 2010. Pyroclastic loss or retention during explosive volcanism on asteroids: Influence of asteroid size and gas content of melt. *Meteoritics & Planetary Science* 45(8):1284-1301.

Yamaguichi A., Takeda H., Bogard D. D., and Garrison D. 1994. Textural variation and impact history of the Millbillillie eucrite. *Meteoritics* 29:237-245.

# APPENDICES

**APPENDIX A.**
**Electron Microprobe analyses of glasses – Weight percent (wt%)**

**EET87532,13**

| Point | glass 4ii | 4v | 4vi | 4vii | 4i_2 | 4ii_2 | 4iii_2 | 4iv_2 | 4v_2 | 4vi_2 | 4vii_2 | 4viii | 4ix |
|---|---|---|---|---|---|---|---|---|---|---|---|---|---|
| $SiO_2$ | 47.5 | 48.2 | 48.2 | 47.8 | 47.7 | 47.8 | 47.5 | 48.1 | 47.9 | 48.0 | 47.5 | 48.0 | 47.4 |
| $TiO_2$ | 0.10 | 0.11 | 0.16 | 0.27 | 0.21 | 0.21 | 0.22 | 0.18 | 0.14 | 0.17 | 0.20 | 0.20 | 0.17 |
| $Al_2O_3$ | 14.4 | 14.7 | 12.3 | 11.9 | 13.2 | 13.2 | 13.0 | 12.9 | 13.4 | 12.3 | 12.8 | 12.8 | 14.0 |
| $Cr_2O_3$ | 0.10 | 0.22 | 0.51 | 1.28 | 0.83 | 0.73 | 0.81 | 0.49 | 0.53 | 0.87 | 0.72 | 0.44 | 0.64 |
| MgO | 9.32 | 9.48 | 10.4 | 10.4 | 9.83 | 9.61 | 10.1 | 10.3 | 10.0 | 10.4 | 10.2 | 10.1 | 9.59 |
| CaO | 11.7 | 11.3 | 10.4 | 9.33 | 11.7 | 12.4 | 10.3 | 10.5 | 10.8 | 11.2 | 9.8 | 11.7 | 10.7 |
| MnO | 0.46 | 0.45 | 0.59 | 0.60 | 0.47 | 0.48 | 0.54 | 0.53 | 0.50 | 0.52 | 0.57 | 0.49 | 0.48 |
| FeO | 15.4 | 15.5 | 18.0 | 19.0 | 15.9 | 15.6 | 17.4 | 17.5 | 16.7 | 16.9 | 17.8 | 16.6 | 16.8 |
| $Na_2O$ | 0.11 | 0.13 | 0.13 | 0.08 | 0.11 | 0.11 | 0.10 | 0.09 | 0.10 | 0.10 | <0.06 | 0.09 | 0.12 |
| $K_2O$ | <0.04 | <0.04 | <0.04 | <0.04 | <0.04 | <0.04 | <0.04 | <0.04 | <0.04 | <0.04 | <0.04 | <0.04 | <0.04 |
| Total | 99.5 | 100.4 | 100.9 | 101.0 | 99.9 | 100.1 | 99.9 | 100.5 | 100.0 | 100.4 | 99.6 | 100.3 | 99.9 |

| Point | glass 4x | 4xi | 8aiii | 8aiv | 8avi | 8ai_2 | 8aii_2 | 8aiii_2 | 8aiv_2 | 8av_2 | 8avi_2 | 8avii |
|---|---|---|---|---|---|---|---|---|---|---|---|---|
| $SiO_2$ | 48.0 | 48.0 | 47.5 | 47.0 | 46.9 | 47.4 | 47.3 | 47.2 | 47.4 | 47.2 | 46.8 | 47.4 |
| $TiO_2$ | 0.16 | 0.14 | 0.81 | 0.81 | 0.90 | 0.75 | 0.85 | 0.87 | 0.85 | 0.85 | 0.85 | 1.01 |
| $Al_2O_3$ | 12.7 | 13.7 | 10.8 | 11.6 | 11.5 | 11.8 | 11.6 | 11.5 | 12.2 | 11.7 | 11.6 | 11.9 |
| $Cr_2O_3$ | 0.74 | 0.35 | 0.73 | 0.46 | 0.68 | 0.50 | 0.49 | 0.66 | 0.63 | 0.60 | 0.80 | 0.50 |
| MgO | 10.1 | 9.83 | 8.39 | 8.28 | 8.12 | 8.22 | 8.36 | 8.36 | 7.81 | 8.55 | 8.23 | 8.19 |
| CaO | 11.4 | 11.0 | 16.5 | 14.2 | 15.4 | 15.9 | 16.4 | 16.0 | 15.2 | 15.7 | 15.8 | 16.4 |
| MnO | 0.48 | 0.49 | 0.43 | 0.47 | 0.49 | 0.44 | 0.47 | 0.48 | 0.43 | 0.51 | 0.46 | 0.43 |
| FeO | 16.6 | 16.7 | 15.1 | 15.3 | 15.5 | 14.6 | 14.5 | 14.8 | 14.6 | 15.2 | 14.9 | 14.3 |
| $Na_2O$ | 0.11 | 0.11 | 0.17 | 0.19 | 0.14 | 0.17 | 0.15 | 0.13 | 0.17 | 0.15 | 0.17 | 0.14 |
| $K_2O$ | <0.04 | <0.04 | <0.04 | <0.04 | <0.04 | <0.04 | <0.04 | <0.04 | <0.04 | <0.04 | <0.04 | <0.04 |
| Total | 100.2 | 100.3 | 100.9 | 98.8 | 100.2 | 99.8 | 100.1 | 100.0 | 99.3 | 100.4 | 99.6 | 100.3 |

**APPENDIX A. Continued**

**QUE94200,16**

| Point | glass 5ci | 5cii | 5ciii | 5civ | 5cv | 5cvi | 5cvii | 5cviii | 6i | 6ii | 6iii | 6iv | 6v |
|---|---|---|---|---|---|---|---|---|---|---|---|---|---|
| $SiO_2$ | 48.3 | 48.8 | 49.2 | 49.5 | 48.8 | 49.0 | 48.9 | 48.6 | 49.4 | 49.3 | 49.0 | 49.1 | 48.7 |
| $TiO_2$ | 0.73 | 0.68 | 0.67 | 0.62 | 0.69 | 0.72 | 0.66 | 0.73 | 0.57 | 0.56 | 0.68 | 0.59 | 0.48 |
| $Al_2O_3$ | 12.4 | 12.2 | 12.2 | 12.0 | 11.9 | 12.2 | 12.6 | 12.0 | 12.0 | 12.2 | 12.0 | 12.4 | 11.4 |
| $Cr_2O_3$ | 0.40 | 0.28 | 0.20 | 0.19 | 0.21 | 0.25 | 0.23 | 0.31 | 0.12 | 0.13 | 0.61 | 0.58 | 0.18 |
| MgO | 13.0 | 12.8 | 12.5 | 13.4 | 12.9 | 13.1 | 13.0 | 12.9 | 13.7 | 13.6 | 13.0 | 12.7 | 13.4 |
| CaO | 14.8 | 14.4 | 14.6 | 13.6 | 14.5 | 14.6 | 14.3 | 15.2 | 11.2 | 11.6 | 12.7 | 13.2 | 12.2 |
| MnO | 0.34 | 0.33 | 0.34 | 0.32 | 0.34 | 0.31 | 0.36 | 0.32 | 0.38 | 0.41 | 0.38 | 0.32 | 0.40 |
| FeO | 9.90 | 10.1 | 9.16 | 10.3 | 10.1 | 9.68 | 9.81 | 9.25 | 12.1 | 11.9 | 11.3 | 11.1 | 12.4 |
| $Na_2O$ | 0.18 | 0.08 | 0.11 | 0.13 | 0.12 | 0.13 | 0.11 | 0.07 | 0.10 | 0.12 | 0.13 | 0.17 | 0.16 |
| $K_2O$ | <0.04 | 0.05 | <0.04 | <0.04 | <0.04 | 0.04 | <0.04 | <0.04 | <0.04 | <0.04 | <0.04 | <0.04 | <0.04 |
| Total | 100.5 | 100.1 | 99.4 | 100.5 | 100.0 | 100.4 | 99.9 | 99.3 | 100.0 | 100.2 | 100.3 | 100.7 | 99.7 |

| Point | glass 6vi | 6vii | 6i_2 | 6ii_2 | 6iii_2 | 6vi_2 | 6vii_2 | 6viii | 6ix | 6x | 6xi | 6xii | 6xiii |
|---|---|---|---|---|---|---|---|---|---|---|---|---|---|
| $SiO_2$ | 49.2 | 49.3 | 49.1 | 49.3 | 49.1 | 48.5 | 49.3 | 49.5 | 49.3 | 49.2 | 49.2 | 48.6 | 49.3 |
| $TiO_2$ | 0.44 | 0.65 | 0.55 | 0.52 | 0.61 | 0.73 | 0.63 | 0.52 | 0.55 | 0.51 | 0.56 | 0.69 | 0.53 |
| $Al_2O_3$ | 12.2 | 12.1 | 12.1 | 11.8 | 12.0 | 12.3 | 12.5 | 12.2 | 12.2 | 12.1 | 12.2 | 12.0 | 12.1 |
| $Cr_2O_3$ | 0.24 | 0.16 | 0.40 | 0.17 | 0.45 | 0.32 | 0.38 | 0.18 | 0.18 | 0.26 | 0.25 | 0.71 | 0.20 |
| MgO | 13.9 | 13.8 | 13.7 | 14.2 | 13.3 | 13.6 | 13.6 | 13.9 | 13.9 | 13.8 | 13.7 | 13.0 | 14.0 |
| CaO | 10.6 | 11.5 | 11.9 | 10.5 | 12.6 | 12.2 | 11.5 | 11.4 | 11.1 | 11.0 | 11.6 | 12.9 | 11.0 |
| MnO | 0.41 | 0.41 | 0.36 | 0.39 | 0.34 | 0.39 | 0.39 | 0.39 | 0.40 | 0.36 | 0.40 | 0.34 | 0.37 |
| FeO | 13.3 | 12.2 | 12.1 | 13.1 | 11.4 | 11.7 | 12.2 | 12.3 | 12.5 | 12.5 | 12.2 | 11.5 | 12.4 |
| $Na_2O$ | 0.15 | 0.12 | 0.12 | 0.12 | 0.11 | <0.06 | 0.13 | 0.11 | 0.13 | 0.13 | 0.13 | 0.15 | 0.12 |
| $K_2O$ | <0.04 | <0.04 | <0.04 | <0.04 | <0.04 | <0.04 | <0.04 | <0.04 | <0.04 | <0.04 | <0.04 | <0.04 | <0.04 |
| Total | 100.8 | 100.7 | 100.4 | 100.1 | 99.9 | 99.8 | 100.6 | 100.5 | 100.2 | 100.0 | 100.2 | 99.8 | 100.1 |

**APPENDIX A. Continued**

| Point | glass 7ci | 7cii | 7ciii | 7civ | 7cv | 7cvi | 7cvii | 15i | 15ii | 15iii | 15iv | 15v | 15vi |
|---|---|---|---|---|---|---|---|---|---|---|---|---|---|
| $SiO_2$ | 48.7 | 48.7 | 48.6 | 49.1 | 49.0 | 49.1 | 48.9 | 47.0 | 47.9 | 47.3 | 48.0 | 48.1 | 47.9 |
| $TiO_2$ | 0.43 | 0.59 | 0.62 | 0.62 | 0.63 | 0.73 | 0.56 | 0.95 | 0.74 | 0.71 | 0.74 | 0.59 | 0.64 |
| $Al_2O_3$ | 12.2 | 12.3 | 11.9 | 11.7 | 12.4 | 11.0 | 12.6 | 11.97 | 12.46 | 12.4 | 12.6 | 12.5 | 12.6 |
| $Cr_2O_3$ | 0.47 | 0.70 | 0.32 | 0.28 | 0.25 | 0.53 | 0.36 | 1.04 | 0.35 | 0.87 | 0.25 | 0.18 | 0.16 |
| MgO | 14.2 | 13.2 | 13.2 | 13.5 | 13.2 | 13.7 | 13.1 | 12.5 | 12.5 | 12.9 | 13.0 | 13.0 | 13.2 |
| CaO | 11.1 | 13.4 | 14.3 | 14.2 | 14.3 | 14.9 | 13.5 | 13.8 | 14.1 | 13.2 | 13.1 | 12.7 | 12.0 |
| MnO | 0.39 | 0.36 | 0.36 | 0.34 | 0.33 | 0.31 | 0.36 | 0.38 | 0.37 | 0.40 | 0.34 | 0.37 | 0.38 |
| FeO | 11.2 | 11.1 | 10.4 | 10.6 | 10.5 | 10.3 | 10.9 | 11.1 | 10.6 | 11.3 | 11.2 | 11.3 | 11.9 |
| $Na_2O$ | 0.10 | 0.10 | 0.12 | 0.10 | 0.08 | <0.06 | 0.09 | 0.19 | 0.08 | 0.17 | 0.18 | 0.15 | 0.17 |
| $K_2O$ | <0.04 | <0.04 | <0.04 | <0.04 | <0.04 | <0.04 | <0.04 | <0.04 | <0.04 | 0.04 | <0.04 | <0.04 | 0.05 |
| Total | 99.0 | 100.7 | 100.1 | 100.7 | 100.8 | 100.8 | 100.6 | 99.3 | 99.4 | 99.5 | 99.6 | 99.2 | 99.3 |

| Point | glass 15vii | 15viii | 15ix | 15x | 15i_2 | 15ii_2 | 15iii_2 | 15viii_2 | 15ix_2 | 15x_2 | 15xi | 15xii | 15xiii |
|---|---|---|---|---|---|---|---|---|---|---|---|---|---|
| $SiO_2$ | 48.1 | 47.6 | 47.7 | 47.9 | 48.0 | 48.1 | 47.9 | 48.4 | 48.1 | 48.1 | 48.1 | 47.6 | 48.0 |
| $TiO_2$ | 0.61 | 0.81 | 0.71 | 0.74 | 0.78 | 0.93 | 0.79 | 0.64 | 0.99 | 0.73 | 0.70 | 0.76 | 0.77 |
| $Al_2O_3$ | 12.8 | 12.2 | 12.4 | 12.6 | 12.6 | 12.4 | 12.4 | 12.5 | 12.2 | 12.2 | 12.4 | 12.5 | 12.4 |
| $Cr_2O_3$ | 0.14 | 0.61 | 0.45 | 0.12 | 0.40 | 0.40 | 0.57 | 0.15 | 0.29 | 0.42 | 0.36 | 0.47 | 0.49 |
| MgO | 13.8 | 12.9 | 13.0 | 13.0 | 12.8 | 12.7 | 12.9 | 13.0 | 13.2 | 13.1 | 12.7 | 13.0 | 12.8 |
| CaO | 10.3 | 13.4 | 12.7 | 11.8 | 13.5 | 13.8 | 12.6 | 12.7 | 12.2 | 12.5 | 13.6 | 12.2 | 13.3 |
| MnO | 0.40 | 0.37 | 0.34 | 0.36 | 0.32 | 0.39 | 0.36 | 0.36 | 0.40 | 0.38 | 0.33 | 0.37 | 0.35 |
| FeO | 13.0 | 11.2 | 11.3 | 11.7 | 10.9 | 10.8 | 11.6 | 11.4 | 11.9 | 11.9 | 10.6 | 11.9 | 11.2 |
| $Na_2O$ | 0.12 | 0.20 | 0.15 | 0.20 | 0.15 | 0.18 | 0.14 | 0.17 | 0.17 | 0.15 | 0.16 | 0.16 | 0.17 |
| $K_2O$ | <0.04 | <0.04 | <0.04 | <0.04 | <0.04 | <0.04 | <0.04 | <0.04 | <0.04 | <0.04 | <0.04 | <0.04 | <0.04 |
| Total | 99.2 | 99.5 | 99.0 | 98.7 | 99.4 | 99.7 | 99.3 | 99.4 | 99.5 | 99.5 | 98.9 | 98.9 | 99.4 |

**APPENDIX A. Continued**

| Point | glass 15xiv | 15xv | 15xvi | 15xvii | 19di | 19dii | 19diii | 19div | 19dv | 19dvi | 19dvii | 19di_2 | 19diii_2 |
|---|---|---|---|---|---|---|---|---|---|---|---|---|---|
| $SiO_2$ | 48.3 | 47.9 | 48.1 | 48.5 | 48.5 | 48.4 | 48.4 | 47.7 | 48.3 | 48.8 | 48.7 | 48.3 | 48.6 |
| $TiO_2$ | 0.73 | 0.73 | 0.82 | 0.64 | 0.61 | 0.60 | 0.50 | 0.55 | 0.51 | 0.47 | 0.59 | 0.56 | 0.58 |
| $Al_2O_3$ | 12.8 | 12.4 | 12.3 | 12.5 | 10.7 | 10.4 | 10.8 | 11.0 | 10.8 | 11.0 | 10.8 | 10.5 | 10.7 |
| $Cr_2O_3$ | 0.17 | 0.35 | 0.31 | 0.14 | 0.37 | 0.51 | 0.30 | 0.25 | 0.41 | 0.22 | 0.26 | 0.32 | 0.31 |
| MgO | 12.8 | 12.6 | 12.6 | 13.5 | 15.2 | 15.3 | 15.2 | 15.3 | 15.1 | 15.6 | 15.0 | 15.4 | 15.1 |
| CaO | 13.1 | 13.9 | 13.7 | 11.8 | 11.2 | 11.0 | 11.2 | 10.4 | 11.1 | 9.5 | 11.1 | 10.8 | 11.2 |
| MnO | 0.34 | 0.34 | 0.36 | 0.39 | 0.38 | 0.35 | 0.38 | 0.40 | 0.38 | 0.44 | 0.41 | 0.39 | 0.37 |
| FeO | 11.1 | 10.7 | 10.7 | 12.1 | 11.8 | 12.1 | 11.9 | 12.6 | 12.2 | 12.7 | 12.0 | 12.1 | 11.9 |
| $Na_2O$ | 0.15 | 0.12 | 0.17 | 0.13 | 0.08 | 0.10 | 0.11 | 0.15 | 0.14 | 0.12 | 0.10 | 0.11 | 0.11 |
| $K_2O$ | <0.04 | 0.05 | <0.04 | <0.04 | <0.04 | <0.04 | 0.04 | <0.04 | 0.04 | <0.04 | <0.04 | <0.04 | <0.04 |
| Total | 99.6 | 99.0 | 99.1 | 99.7 | 99.0 | 99.0 | 98.9 | 98.5 | 99.3 | 99.0 | 99.2 | 98.6 | 98.9 |

**MIL05805,2**

| Point | glass 1ai | 1aii | 1aiv | 1av | 1avi | 1avii | 1aii_2 | 1aiii_2 | 1aiv_2 | 1av_2 | 1avi_2 | 1aviii | 1aix |
|---|---|---|---|---|---|---|---|---|---|---|---|---|---|
| $SiO_2$ | 51.3 | 52.5 | 51.9 | 51.9 | 52.7 | 52.5 | 52.3 | 52.3 | 52.2 | 51.9 | 52.5 | 52.1 | 52.1 |
| $TiO_2$ | 0.24 | 0.18 | 0.21 | 0.32 | 0.21 | 0.20 | 0.32 | 0.32 | 0.29 | 0.34 | 0.35 | 0.34 | 0.31 |
| $Al_2O_3$ | 5.18 | 5.48 | 5.64 | 5.60 | 5.89 | 5.79 | 5.56 | 5.48 | 5.80 | 5.61 | 5.66 | 5.51 | 5.74 |
| $Cr_2O_3$ | 0.44 | 0.82 | 0.76 | 0.56 | 0.70 | 0.96 | 0.76 | 0.70 | 0.76 | 0.52 | 0.68 | 0.64 | 0.78 |
| MgO | 20.6 | 20.4 | 20.4 | 19.0 | 19.0 | 18.5 | 20.7 | 19.8 | 20.2 | 19.0 | 19.4 | 19.3 | 19.9 |
| CaO | 3.00 | 5.36 | 3.21 | 3.04 | 3.03 | 3.17 | 4.98 | 3.33 | 3.10 | 3.08 | 3.09 | 2.99 | 3.23 |
| MnO | 0.37 | 0.50 | 0.35 | 0.34 | 0.25 | 0.26 | 0.46 | 0.35 | 0.37 | 0.34 | 0.30 | 0.35 | 0.33 |
| FeO | 17.5 | 14.5 | 16.3 | 18.0 | 16.5 | 17.1 | 14.6 | 16.7 | 15.6 | 18.1 | 16.9 | 17.7 | 16.1 |
| $Na_2O$ | 0.16 | 0.07 | 0.17 | 0.11 | 0.18 | 0.17 | 0.06 | 0.16 | 0.18 | 0.16 | 0.16 | 0.19 | 0.19 |
| $K_2O$ | 0.88 | <0.04 | 0.83 | 1.36 | 1.01 | 1.03 | 0.23 | 1.08 | 1.13 | 1.12 | 1.20 | 1.12 | 1.16 |
| Total | 99.9 | 100.2 | 100.3 | 100.9 | 99.5 | 100.1 | 100.0 | 100.2 | 99.7 | 100.1 | 100.3 | 100.3 | 99.9 |

**APPENDIX A. Continued**

| Point | glass 1ax | 1axi | 1axii | 1axiii | 1axiv | 1axv | 1axvi | 1axvii | 1axviii |
|---|---|---|---|---|---|---|---|---|---|
| $SiO_2$ | 52.5 | 52.3 | 52.8 | 52.3 | 52.7 | 52.2 | 52.2 | 52.6 | 52.5 |
| $TiO_2$ | 0.33 | 0.29 | 0.35 | 0.36 | 0.31 | 0.30 | 0.32 | 0.33 | 0.34 |
| $Al_2O_3$ | 5.76 | 5.62 | 5.90 | 5.58 | 5.81 | 5.48 | 5.64 | 5.55 | 5.55 |
| $Cr_2O_3$ | 0.84 | 0.70 | 0.76 | 0.79 | 0.66 | 0.75 | 0.76 | 0.77 | 0.81 |
| MgO | 20.1 | 20.6 | 19.8 | 19.6 | 18.8 | 20.4 | 20.0 | 20.4 | 20.1 |
| CaO | 3.19 | 3.19 | 3.38 | 3.15 | 3.16 | 3.12 | 5.49 | 5.07 | 5.35 |
| MnO | 0.37 | 0.39 | 0.34 | 0.34 | 0.33 | 0.39 | 0.48 | 0.49 | 0.44 |
| FeO | 15.4 | 16.0 | 15.8 | 16.2 | 17.1 | 16.3 | 14.6 | 14.5 | 14.4 |
| $Na_2O$ | 0.15 | 0.15 | 0.16 | 0.17 | 0.20 | 0.14 | 0.09 | 0.07 | 0.08 |
| $K_2O$ | 1.14 | 1.08 | 1.14 | 1.17 | 1.24 | 1.12 | 0.23 | 0.30 | 0.28 |
| Total | 99.8 | 100.3 | 100.5 | 99.8 | 100.3 | 100.3 | 99.8 | 100.0 | 99.8 |

**MIL05805,11**

| Point | glass 1i | 1ii | 1iii | 1iv | 1v | 1vi | 1vii | 1ii_2 | 1iii_2 | 1iv_2 | 1v_2 | 1viii | 1ix |
|---|---|---|---|---|---|---|---|---|---|---|---|---|---|
| $SiO_2$ | 50.3 | 50.0 | 50.6 | 49.9 | 50.1 | 50.5 | 50.4 | 49.7 | 49.6 | 49.6 | 49.7 | 50.0 | 49.4 |
| $TiO_2$ | 0.52 | 0.53 | 0.59 | 0.57 | 0.59 | 0.56 | 0.58 | 0.53 | 0.56 | 0.53 | 0.53 | 0.49 | 0.51 |
| $Al_2O_3$ | 9.49 | 9.48 | 9.49 | 9.38 | 9.49 | 9.42 | 9.47 | 9.26 | 9.26 | 9.34 | 9.34 | 9.27 | 9.25 |
| $Cr_2O_3$ | 0.73 | 0.68 | 0.70 | 0.60 | 0.63 | 0.71 | 0.70 | 0.68 | 0.66 | 0.65 | 0.64 | 0.68 | 0.62 |
| MgO | 12.2 | 12.3 | 12.1 | 12.0 | 11.7 | 12.0 | 12.2 | 12.6 | 12.5 | 12.2 | 12.1 | 12.4 | 12.5 |
| CaO | 7.55 | 7.29 | 6.32 | 7.04 | 7.70 | 7.69 | 7.72 | 7.49 | 6.47 | 7.43 | 7.50 | 7.55 | 7.36 |
| MnO | 0.53 | 0.61 | 0.64 | 0.62 | 0.58 | 0.52 | 0.54 | 0.56 | 0.58 | 0.55 | 0.57 | 0.53 | 0.63 |
| FeO | 17.7 | 18.5 | 18.6 | 18.3 | 18.3 | 18.1 | 18.0 | 17.2 | 18.5 | 17.9 | 18.0 | 17.5 | 18.0 |
| $Na_2O$ | 0.16 | 0.14 | 0.13 | 0.16 | 0.15 | 0.13 | 0.14 | 0.15 | 0.20 | 0.19 | 0.11 | 0.17 | 0.11 |
| $K_2O$ | 0.83 | 0.72 | 0.84 | 0.78 | 0.86 | 0.80 | 0.89 | 0.78 | 0.86 | 0.86 | 0.78 | 0.75 | 0.80 |
| Total | 100.0 | 100.2 | 100.0 | 99.4 | 100.1 | 100.5 | 100.6 | 99.0 | 99.2 | 99.3 | 99.3 | 99.2 | 99.1 |

**APPENDIX A. Continued**

| Point | glass 1x | 1xi | 1xii | 1xiii | 2i | 2ii | 2iii | 2iv | 2v | 7i | 7ii | 7iii | 7iv |
|---|---|---|---|---|---|---|---|---|---|---|---|---|---|
| $SiO_2$ | 50.1 | 49.6 | 49.5 | 49.1 | 49.1 | 48.4 | 48.7 | 48.7 | 48.2 | 50.2 | 50.0 | 50.3 | 50.5 |
| $TiO_2$ | 0.56 | 0.55 | 0.52 | 0.52 | 0.68 | 0.63 | 0.70 | 0.60 | 0.63 | 0.86 | 0.82 | 0.81 | 0.88 |
| $Al_2O_3$ | 9.21 | 9.29 | 9.24 | 9.27 | 11.9 | 11.7 | 11.6 | 11.6 | 11.5 | 11.0 | 11.6 | 10.4 | 11.0 |
| $Cr_2O_3$ | 0.66 | 0.66 | 0.61 | 0.63 | 0.37 | 0.47 | 0.45 | 0.40 | 0.44 | 0.34 | 0.37 | 0.36 | 0.35 |
| MgO | 12.5 | 12.3 | 12.3 | 12.1 | 8.54 | 8.74 | 8.95 | 8.53 | 8.82 | 8.03 | 7.50 | 8.45 | 8.18 |
| CaO | 7.26 | 7.35 | 7.49 | 7.88 | 7.68 | 9.81 | 7.94 | 9.36 | 11.82 | 9.01 | 10.19 | 8.99 | 8.46 |
| MnO | 0.58 | 0.57 | 0.57 | 0.58 | 0.52 | 0.55 | 0.56 | 0.57 | 0.59 | 0.56 | 0.52 | 0.58 | 0.65 |
| FeO | 17.9 | 17.8 | 18.0 | 18.2 | 19.4 | 19.2 | 19.9 | 18.9 | 18.0 | 18.7 | 17.6 | 18.9 | 19.1 |
| $Na_2O$ | 0.17 | 0.13 | 0.12 | 0.14 | 0.21 | 0.22 | 0.20 | 0.22 | 0.14 | 0.24 | 0.23 | 0.21 | 0.24 |
| $K_2O$ | 0.86 | 0.76 | 0.80 | 0.74 | 1.15 | 1.00 | 0.99 | 1.14 | 0.47 | 1.20 | 1.43 | 1.16 | 1.18 |
| Total | 99.7 | 99.0 | 99.1 | 99.2 | 99.6 | 100.7 | 100.1 | 100.1 | 100.6 | 100.1 | 100.3 | 100.1 | 100.6 |

| Point | glass 7v | 7vi | 7i_2 | 7iv_2 | 7v_2 | 7vi_2 | 7xi | 7xii | 7xiii | 7xiv | 7xv | 7xvi | 7xvii |
|---|---|---|---|---|---|---|---|---|---|---|---|---|---|
| $SiO_2$ | 50.0 | 49.0 | 49.9 | 49.5 | 49.4 | 50.1 | 49.8 | 48.0 | 49.3 | 49.5 | 50.0 | 49.4 | 49.0 |
| $TiO_2$ | 0.83 | 0.92 | 0.76 | 0.70 | 0.78 | 0.72 | 0.74 | 0.69 | 0.81 | 0.71 | 0.76 | 0.77 | 0.77 |
| $Al_2O_3$ | 11.4 | 11.7 | 11.0 | 10.3 | 11.4 | 11.9 | 11.5 | 12.9 | 11.2 | 12.2 | 11.5 | 11.2 | 11.3 |
| $Cr_2O_3$ | 0.35 | 0.37 | 0.35 | 0.39 | 0.36 | 0.37 | 0.36 | 0.38 | 0.39 | 0.39 | 0.36 | 0.39 | 0.38 |
| MgO | 7.86 | 7.97 | 8.02 | 8.33 | 8.16 | 7.70 | 7.87 | 7.73 | 8.09 | 7.57 | 7.80 | 7.99 | 8.12 |
| CaO | 9.88 | 10.78 | 8.72 | 9.51 | 9.43 | 9.62 | 9.21 | 10.61 | 9.07 | 8.67 | 9.11 | 9.53 | 9.85 |
| MnO | 0.54 | 0.54 | 0.56 | 0.58 | 0.55 | 0.49 | 0.56 | 0.53 | 0.58 | 0.57 | 0.56 | 0.52 | 0.54 |
| FeO | 17.6 | 17.6 | 18.5 | 18.1 | 17.8 | 16.8 | 17.5 | 16.9 | 18.0 | 17.7 | 17.2 | 17.6 | 17.6 |
| $Na_2O$ | 0.28 | 0.21 | 0.27 | 0.18 | 0.25 | 0.27 | 0.25 | 0.22 | 0.23 | 0.27 | 0.32 | 0.22 | 0.22 |
| $K_2O$ | 1.33 | 1.07 | 1.17 | 1.16 | 1.18 | 1.39 | 1.26 | 1.14 | 1.20 | 1.25 | 1.40 | 1.19 | 1.18 |
| Total | 100.1 | 100.2 | 99.2 | 98.7 | 99.3 | 99.3 | 99.1 | 99.1 | 98.8 | 98.8 | 99.0 | 98.8 | 98.9 |

**APPENDIX B.**
**LA-ICP-MS analyses of glasses – Parts per million (ppm)**

| | QUE94200,16 | | | | | | | |
|---|---|---|---|---|---|---|---|---|
| Point | 5c | 6 | 7c | 15_1 | 15_2 | 15_3 | 15_4 | 19d |
| Na | 862.7 | 1,430.2 | 617.6 | 2003.1 | 2097.1 | 1203.8 | 1111.6 | 842.2 |
| K | 138.2 | 74,193.5 | 129.3 | 283.9 | 312.2 | 200.8 | 188.8 | 145.7 |
| Co | n.d. | 43.733 | n.d. | 185.541 | 311.622 | n.d. | n.d. | n.d. |
| Ni | n.d. | 184.09 | 12.456 | 752.47 | 1,239.18 | n.d. | n.d. | 17.093 |
| Zn | 2.688 | n.d. | n.d. | 3.012 | n.d. | n.d. | n.d. | n.d. |
| Rb | 9.294 | n.d. | 0.963 | 8.062 | 7.481 | 4.244 | 1.929 | 2.783 |
| Y | 15.751 | 14.029 | 16.53 | 11.493 | 13.183 | 15.279 | 14.943 | 14.412 |
| Cd | n.d. | 0.797 | n.d. | n.d. | n.d. | n.d. | n.d. | n.d. |
| La | 3.082 | 2.971 | 3.494 | 2.858 | 2.951 | 3.304 | 3.506 | 2.828 |
| Nd | 6.188 | 5.344 | 7.757 | 4.820 | 6.834 | 6.587 | 6.736 | 5.074 |
| Sm | 2.042 | 1.320 | 2.113 | 1.109 | 2.159 | 2.014 | 1.923 | 1.537 |
| Eu | 0.679 | 0.705 | 0.619 | 0.633 | 0.600 | 0.744 | 0.672 | 0.583 |
| Gd | 2.771 | 2.423 | 2.611 | 1.537 | 1.457 | 3.371 | 2.873 | 2.261 |
| Dy | 2.914 | 2.428 | 2.953 | 2.198 | 2.335 | 2.888 | 3.085 | 2.416 |
| Ho | 0.659 | 0.590 | 0.628 | 0.407 | 0.524 | 0.44 | 0.566 | 0.429 |
| Tm | 0.204 | 0.268 | 0.310 | 0.167 | 0.161 | 0.259 | 0.216 | 0.175 |
| Lu | n.d. | n.d. | 0.225 | n.d. | n.d. | n.d. | n.d. | n.d. |
| Hf | 1.017 | 1.150 | 0.993 | 1.054 | 1.719 | 1.16 | 0.857 | 1.085 |
| Ta | 0.160 | 0.153 | 0.171 | 0.126 | 0.151 | 0.157 | 0.213 | 0.136 |
| Pb | 0.427 | 0.240 | 0.376 | 0.389 | 0.385 | 0.413 | 0.428 | 0.304 |
| Th | 0.364 | 0.388 | 0.382 | 0.444 | 0.327 | 0.376 | 0.246 | 0.377 |
| U | 0.086 | 0.081 | 0.071 | 0.080 | 0.110 | 0.077 | 0.056 | 0.077 |

**APPENDIX B. Continued**

| | MIL05805,2 | | | | MIL05805,11 | | | | | |
|---|---|---|---|---|---|---|---|---|---|---|
| Point | 1a_1 | 1a_2 | 1a_3 | Point | 1_1 | 1_2 | 2 | 7_1 | 7_2 | 7_3 |
| Na | 1,139.2 | 1,169.5 | 1,132.0 | Na | 1174.0 | 1177.8 | 1728.0 | 1862.6 | 1738.0 | 1762.7 |
| K | 10,046.9 | 10,262.6 | 10,116.1 | K | 7285.2 | 7275.3 | 10284.5 | 11114.8 | 10317.1 | 10512.8 |
| Co | n.d. | 2.548 | 2.891 | Co | 4.225 | 7.512 | 26.682 | 2.888 | n.d. | n.d. |
| Ni | n.d. | 15.618 | 95.735 | Ni | 20.222 | 29.503 | 119.149 | 28.076 | 13.388 | 17.424 |
| Zn | 1.885 | 2.433 | 3.177 | Zn | n.d. | 3.894 | 6.598 | 5.998 | 4.464 | 5.471 |
| Rb | 12.838 | 13.105 | 13.265 | Rb | 8.204 | 8.091 | 10.266 | 12.065 | 11.404 | 11.204 |
| Y | 8.578 | 8.446 | 8.539 | Y | 13.122 | 12.606 | 15.51 | 16.308 | 15.865 | 16.068 |
| Cd | n.d. | n.d. | n.d. | Cd | 0.743 | 0.682 | n.d. | 1.447 | 1.208 | 0.688 |
| La | 1.494 | 1.516 | 1.564 | La | 2.722 | 2.547 | 3.016 | 2.986 | 3.014 | 3.205 |
| Nd | 3.454 | 3.145 | 2.610 | Nd | 5.772 | 4.462 | 6.103 | 6.486 | 5.842 | 5.835 |
| Sm | 0.934 | 1.303 | 0.695 | Sm | 1.116 | 1.957 | 1.782 | 2.096 | 1.869 | 1.906 |
| Eu | 0.36 | 0.336 | 0.464 | Eu | 0.680 | 0.657 | 0.940 | 0.659 | 0.653 | 0.663 |
| Gd | 1.143 | 1.627 | 1.222 | Gd | 1.362 | 2.189 | 2.642 | 2.135 | 2.416 | 1.845 |
| Dy | 1.377 | 1.456 | 1.428 | Dy | 2.320 | 2.132 | 2.775 | 2.865 | 2.488 | 2.806 |
| Ho | 0.340 | 0.310 | 0.342 | Ho | 0.517 | 0.443 | 0.560 | 0.608 | 0.593 | 0.549 |
| Tm | 0.084 | 0.204 | 0.139 | Tm | 0.239 | 0.219 | 0.236 | 0.282 | 0.294 | 0.200 |
| Lu | n.d. | n.d. | 0.177 | Lu | 0.251 | 0.269 | 0.394 | 0.286 | 0.259 | 0.293 |
| Hf | 0.729 | 1.032 | 0.554 | Hf | 1.422 | 0.939 | 1.220 | 1.172 | 1.044 | 1.132 |
| Ta | 0.132 | 0.119 | 0.083 | Ta | 0.178 | 0.169 | 0.159 | 0.128 | 0.126 | 0.156 |
| Pb | 1.097 | 0.912 | 0.313 | Pb | 0.324 | 0.31 | 0.417 | 0.399 | 0.478 | 0.488 |
| Th | 0.208 | 0.228 | 0.205 | Th | 0.366 | 0.313 | 0.429 | 0.327 | 0.358 | 0.405 |
| U | 0.064 | 0.059 | 0.050 | U | 0.071 | 0.089 | 0.103 | 0.112 | 0.080 | 0.104 |

# VITA

Sheryl A. Singerling was born on February 28, 1988 in Stroudsburg, Pennsylvania. At the age of 3, she moved to High Point, North Carolina with her family where she was raised for 15 years. Sheryl graduated from Ragsdale High School in June, 2006. The following Fall, Sheryl moved to Chapel Hill, North Carolina where she attended the University of North Carolina. She graduated with Honors and was awarded a Bachelor of Science degree in Geology in May, 2010. In the Fall of 2010, Sheryl joined the graduate program in the Department of Earth and Planetary Sciences at the University of Tennessee. She completed her Master of Science degree in Geology in August, 2012.